FRACTURE ANALYSIS AND CORROSION FATIGUE IN PIPELINES

by

F. Erdogan and R.P. Wei

Department of Mechanical Engineering and Mechanics

Lehigh University, Bethlehem, PA 18015

September 1983

ANNUAL REPORT

Prepared for

U.S. Department of Transportation

Research and Special Programs Administration

Office of University Research

Under the Contract DTRS 56 82-C-00014

FRACTURE ANALYSIS AND CORROSION FATIGUE IN PIPELINES

by

F. Erdogan and R.P. Wei

Department of Mechanical Engineering and Mechanics

Lehigh University, Bethlehem, PA 18015

September 1983

ANNUAL REPORT

Prepared for

U.S. Department of Transportation

Research and Special Programs Administration

Office of University Research

Under the Contract DTRS 56 82-C-00074

Technical Report Documentation Page

1. Report No.	2. Government Accession No.	3. Recipient's Catalog No.
		5. Report Date: September 1983
		6. Performing Organization Code
7. Author(s): F. Erdogan and R.P. Wei		8. Performing Organization Report No.
9. Performing Organization Name and Address: Department of Mechanical Engineering and Mechanics, Lehigh University, Bethlehem, PA 18015		10. Work Unit No. (TRAIS)
		11. Contract or Grant No.: DTRS 56 82-C-00014
12. Sponsoring Agency Name and Address: U.S. Department of Transportation, Research and Special Programs Administration, Office of University Research, Washington, D.C.		13. Type of Report and Period Covered: Annual Report, October 1982-September 1983
		14. Sponsoring Agency Code

15. Supplementary Notes

16. Abstract

In this report the completed part of the research project on the fracture analysis and corrosion fatigue in pipelines is presented. The report consists of two parts. The first part describes the theoretical work on the flaw evaluation as it relates to weld defects in pipelines. The experimental work on the corrosion fatigue in pipeline steels is discussed in the second part. The fracture mechanics methodology is used throughout the investigation. First, the possible weld defects have been reviewed and classified from a viewpoint of their importance in a fracture initiation and propagation process. Then a group of flaw-flaw and flaw-free surface interaction problems have been identified and investigated. Three groups of defects which are identified are pores and solid inclusions with smooth boundaries, pores, notches, and solid inclusions with sharp corners, and cracks and planar inclusions. The results for the following interaction problems have been presented: the interaction between a crack and a solid inclusion or a pore, between cracks and boundaries, between multiple cracks, between flat inclusions and cracks, and planar cracks of finite size. In the second part of the report after briefly discussing the mechanisms of corrosion fatigue, the electrochemical measurement techniques for determining the kinetics of passivation or surface reaction of clean surfaces are described. The completed part of the studies on the kinetics of corrosion fatigue crack propagation in X70 linepipe

TO BE

17. Key Words	18. Distribution Statement
Fracture Mechanics, Pipelines, Flaw Interaction, Weld Defects, Cracks, Inclusions, Fatigue Crack Propagation, Corrosion Fatigue, Chemical Reactions, Environmental Effects	This document is available to the U.S. public through the National Technical Information Service, Springfield, Virginia 22161

19. Security Classif. (of this report)	20. Security Classif. (of this page)	21. No. of Pages	22. Price
Unclassified	Unclassified		

TABLE OF CONTENTS

Table of Contents - cont.

FRACTURE ANALYSIS AND CORROSION FATIGUE IN PIPELINES

Scope of the Project

The primary objectives of this research program are

(a) Classification and assessment of the relative importance of various types of weld defects

(b) An in-depth study of the problem of interaction between two flaws and between flaws and pipe surfaces

(c) Fracture analysis of pipes with crack arrestors

(d) The effect of crack orientation on the strength of pipes

(e) The development of quantitative understanding of the early stage of chemical reactions in relation to the corrosion fatigue crack initiation and propagation

(f) Elucidating the mechanisms for corrosion fatigue crack initiation and propagation, including the influences of chemical, mechanical and metallurgical variables in pipeline steels

(g) The formulation and evaluation of models for predicting cracking response and service performance by using a combined fracture mechanics, surface chemistry and materials science approach.

In this first annual report the completed part of the research program is described and the results are presented.

General Information

The research presented in this report is supported by the U.S. Department of Transportation, Office of University Research, and by the U.S. Department of Interior, Minerals Management Service. Mr. Duglas B. Chisholm of DOT Research and Special Programs Administration, Office of Pipeline Safety Regulation is the Project Monitor. Dr. Charles

E. Smith, Research Program Manager, Technology Assessment and Research Branch, Minerals Management Service is the Department of Interior technical representative.

Part I of the report describes the theoretical research carried out by Professor F. Erdogan, the Principal Investigator, Mr. B. Aksel and Dr. X-H Liu. Part II presents the experimental work which was carried out by Professor R.P. Wei, the Co-Principal Investigator and Mr. S. Chiou.

FRACTURE ANALYSIS AND CORROSION FATIGUE IN PIPELINES

PART I

THE FLAW INTERACTION STUDIES

In this part of the report various kinds of flaws which may be found in pipelines, particularly in girth welds are classified and the problem of interaction between the stress fields of typical flaws are considered. The emphasis in the study is on the application of fracture mechanics techniques to the problem of flaw evaluation.

1. INTRODUCTION

The standards of acceptability of welds in pipelines are generally based on certain empirical criteria in which primary importance is placed on flaw length. Specifically for girth welds such standards are described in API STANDARD 1104 prepared by the "American Petroleum Institute - American Gas Association Joint Committee on Oil and Gas Pipeline Field Welding Practices". However, the API Standard also recognizes fitness for purpose criteria based on fracture mechanics methodology as an alternative technique for flaw evaluation. The advantage of the fracture mechanics approach is that since it takes into account all factors which may be relevant to the failure of the pipe such as the type and the relative size, shape, orientation and location of the flaw, the effect of multiple flaws, the nature of the applied stresses, and the environmental conditions, it could be somewhat more precise than the empirical rules which are largely based on the flaw length.

In fracture mechanics approach to flaw evaluation it is implicitly assumed that the material contains some macroscopic flaws which may form the nucleus of fracture initiation. Generally, these flaws may be mapped by using an appropriate nondestructive flaw detection technique. Aside from the weld defects the pipe may also have flaws which may be external

in origin. Generally the initial phase of the failure in a pipe is the rupture of the net ligament adjacent to the critical flaw in the pipe wall. In most cases the resulting through crack is arrested and the pipe is repaired before further damage. However, in some cases the resulting through crack, after some stable growth, may become unstable leading to circumferential pipe break or dynamic propagation of an axial crack. The initial rupture of the net ligament in the pipe wall is usually preceded by some subcritical crack growth due to fatigue, corrosion fatigue, or stress corrosion cracking and the actual net ligament rupture is generally a ductile fracture process.

Therefore, it is seen that in order to apply fracture mechanics analysis to welded pipes, first one needs to characterize the material itself (the base metal, the weld material and the material in the heat affected zone) with regard to fatigue and corrosion fatigue crack propagation, stress corrosion cracking, fracture toughness and ductile fracture. Next, for a given flaw geometry and loading conditions one has to solve the related mechanics problem to calculate the appropriate fracture mechanics parameter such as the stress intensity factor, the crack tip opening displacement, or the J-integral. The third step in the process would be the selection or development of a proper failure theory and the application of the related quantitative failure criterion. The type of analysis and the experimental work to be performed and the particular criterion to be used are clearly dependent on the expected or the most likely mode of failure.

Even though the primary applied load in the pipelines is the internal pressure which is largely time-independent, there may be some small variations in pressure and some vibrations particularly near the pumping stations which may add a fluctuating component to the static stresses just high enough to cause concern. There are also secondary stresses which are mainly time-varying in nature and therefore would enhance the subcritical crack propagation. Some of the sources of these secondary stresses are misalignment and fit-up, daily, seasonal and other thermal fluctuations, ground settlement and possible earthquakes, axial constraint,

and gross bending in offshore piping due to buoyancy and other hydro-elastic effects. It should be added that the "stress transients" may also play a major role in the subcritical crack propagation and particularly in the final phase of the fracture process, if one takes place. These stresses are generally caused by the pressure waves resulting from changes in flow rate due to partially or fully closing of the valves. In the case of pipes carrying liquids such as petroleum pipelines this is known as the "water hammer" effect due to which the peak pressure may be as high as multiples of the then operating pressure in the pipe. In the natural gas pipelines, this increase in the peak pressure may be somewhat more moderate. Nevertheless, in either case, such sudden surges of pressure are probably responsible in most cases for the final stage of the net ligament failure in the pipe wall resulting in leaks or in a catastrophic fai1ure.

A detailed description and classification of weld discontinuities (including "flaws" which are considered to be undesirable) and a critical review of the literature as we71 as very extensive references on the subject up to 1976 may be found in [1]. The problem of interaction between two (planar) cracks and some empirical rules to define a single equivalent crack are discussed in [2]. The procedures dealing with the subcritical crack propagation by using the tools of linear elastic fracture mechanics (LEFM) is highly standardized and may be found, for example, in [3] or [4]. Similarly, the process of brittle or quasi-brittle fracture is relatively well-understood and is easily dealt with techniques based on LEFM and the concept of fracture toughness. The process which is not well-understood and not standardized, however, is the ductile fracture. The Appendix in the API Standard 1104 concerning the fracture mechanics applications is based on the critical crack tip opening displacement concept, whereas the J-integral seems to be more widely used in pressure vessel technology. The description, some applications of and extensive references on the crack opening displacement approach to fracture may be found in [5]-[7]. Application of a general fracture instability concept based on the crack opening displacement to shells and plates with a part-through crack is described in [8].

In this report the emphasis is on the flaw evaluation based on fracture mechanics techniques. In particular this part of the study is concerned with the effect flaw-flaw and flaw-boundary interaction on the fracture mechanics parameters. After classifying possible flaws which may be found in welds from a viewpoint of their importance in fracture mechanics applications, some of the more important flaw interaction problems have been identified, their method of solution is briefly discussed and some typical and useful results are given.

2. TYPES OF FLAWS

In this report our primary interest in flaws is from a viewpoint of their influence on enhancing or inhibiting fracture initiation and propagation in the pipe. Generally a flaw may be defined as a discontinuity in material constants or geometry. Variety of inclusions come under first and notches, pores and cracks come under the second group of flaws. A common feature of all flaws is that they disturb or perturb the stress field around them. Generally this perturbation gives rise to a stress concentration around the flaw. However, for certain types of flaws there may also be a reduction in key components of the stresses. With their importance in the application of fracture mechanics analysis in mind, in this study we will, therefore, introduce a somewhat unconventional classification of flaws.

2.1 Pores and Solid Inclusions

Pores are the holes or voids in the material having entirely smooth surfaces (Fig. 1.a1). If σ_0 refers to the magnitude of the uniform stress field outside the perturbation region of the pore, then the pore leads to a stress concentration which is of the form

$$\sigma_{max} = K\sigma_0 , \quad K = \frac{A}{\sqrt{\rho}} , \tag{1}$$

where K is the "stress concentration factor", A is a (finite) constant which depends on the geometry of the medium and ρ is radius of curvature

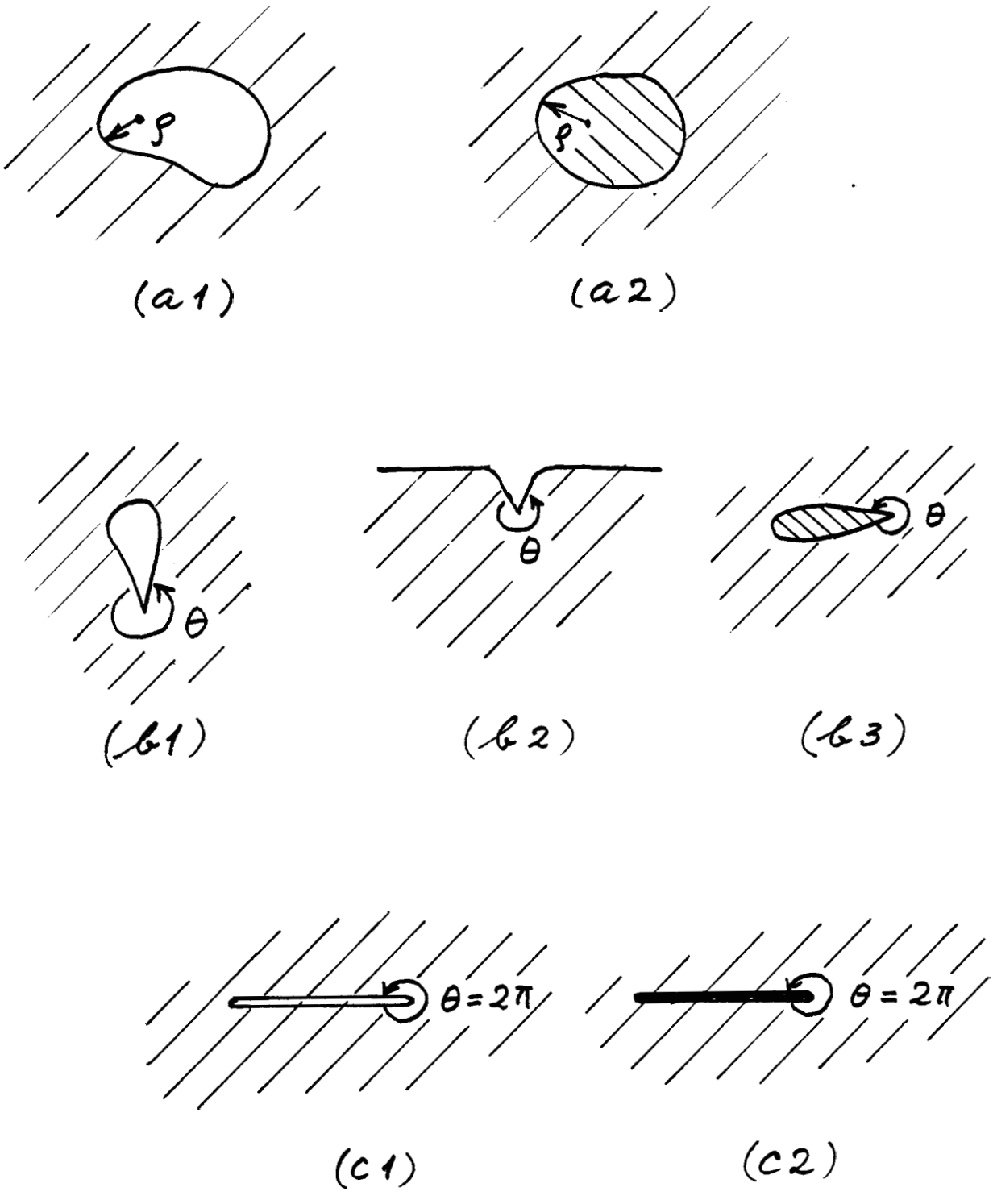

Fig. 1 Types of **Flaws**

of the pore. Generally K is greater than one. We note that surface notches with finite radius of curvature ρ would also come under this category.

Solid inclusions are the second phase materials in the medium also having entirely smooth surfaces. The modulus E_i of the inclusion may be greater or less than the modulus E of the matrix or the base material, the two limiting cases being the rigid inclusion ($E_i=\infty$) and the hole ($E_i=0$). If $E_i<E$, qualitatively the perturbed stress field of the inclusion is similar to that of a pore, meaning that there would be a stress concentration around the inclusion. On the other hand, if $E_i>E$ there would be a reduction in the net section stress. However, in this case there would also be a stress concentration in other planes perpendicular to the applied stress. For example, Fig. 2 shows the stress distribution in a medium containing a circular inclusion under plane strain or plane stress conditions. Note that for c>R around the inclusion there is indeed some stress concentration. In this figure, μ is the shear modulus, $\kappa = 3-4\nu$ for plane strain, and $\kappa = (3-\nu)/(1+\nu)$ for plane stress, ν being the Poisson's ratio.

2.2 Pores, Notches and Solid Inclusions with Sharp Corners

From Eq. (1) and Fig, 2 it may be seen that from a viewpoint of failure analysis a distinguishing feature of the pores, notches and solid inclusions with smooth surfaces is that the stress state around such flaws is always bounded. Eq. (1) also indicates that as the root radius ρ of the notch tends to zero, the stress state around notch tip would tend to infinity, Particularly in problems concerning brittle fracture and fatigue crack initiation such flaws may have to be treated differently. In these nonplanar flaw problems it is said that the inclusion or the notch tip is a point of stress singularity around which the stress state would have the following behavior:

$$\sigma_{ij} = \frac{k}{r^{\lambda}} \quad , \quad 0 < \mathrm{Re}(\lambda) \leq 1/2 \quad , \tag{2}$$

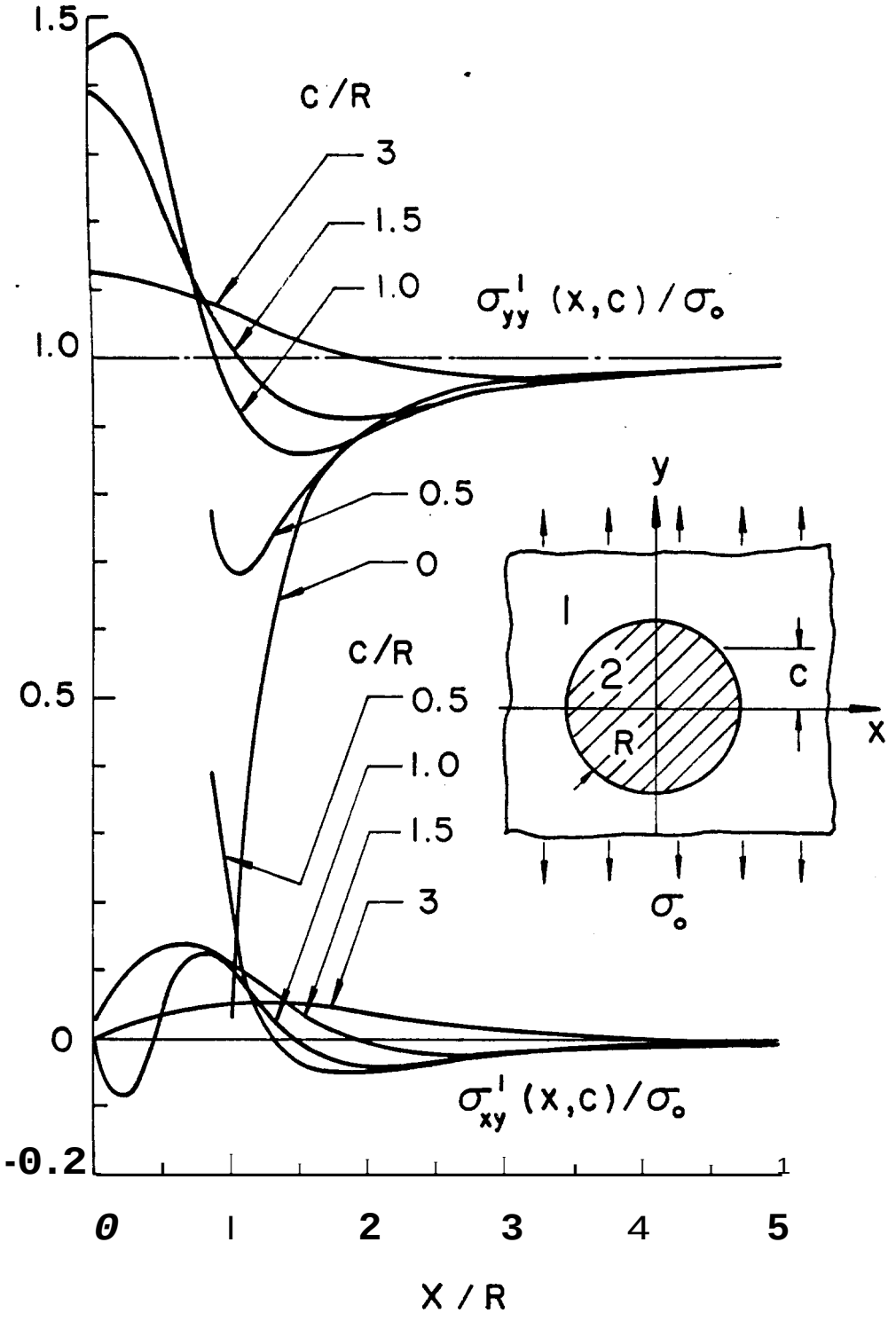

Figure 2. The **stress distribution in a plate with a circular elastic inclusion** ($\mu_2 = 23\mu_1$, $\kappa_1 = 1.6$, $\kappa_2 = 1.8$).

where k and λ are constants representing the strength and the power of the stress singularity and r is a (small) distance from the notch tip. Generally, Eq. (2) is valid for values of the material angle $\theta > \pi$ (Fig. 1 bl , b2, b3). Even though the term "stress intensity factor" is commonly used in relation with crack problems for which $A = 0.5$, in the more general problem leading to an expression such as (2) k is also called the "stress intensity factor".

In the case of notches with a material angle $\pi < \theta < 2\pi$ the power of singularity A is dependent on θ only and may be obtained from (see, for example, [9] where the general problem of bimaterial wedge under variety of boundary conditions are discussed)

$$\cos[2(\lambda-1)\theta] - 1 + (\lambda-1)^2(1-\cos 2\theta) = 0 \quad . \tag{3}$$

Fig. 3 shows the solution of (3) in the relevant range.

2.3 Cracks and Flat Inclusions

These are simply the planar flaws in which the material angle θ (theoretically) is 2π (Fig. 1 cl, c2). Again, the inclusion may be elastic or rigid, the crack being a limiting case with zero modulus. In all planar inclusion as well as crack problems eq. (2) is valid with $A = 0.5$.

The bulk of the material in this report is devoted to the problem of interaction between two flaws or a flaw and a boundary. Since the initial phase of the fracture problem is invariably a subcritical crack growth and since the stress intensity factor is the primary fracture mechanics parameter used in analyzing the subcritical crack growth process, the quantitative results in the interaction problems considered are mostly the stress intensity factors.

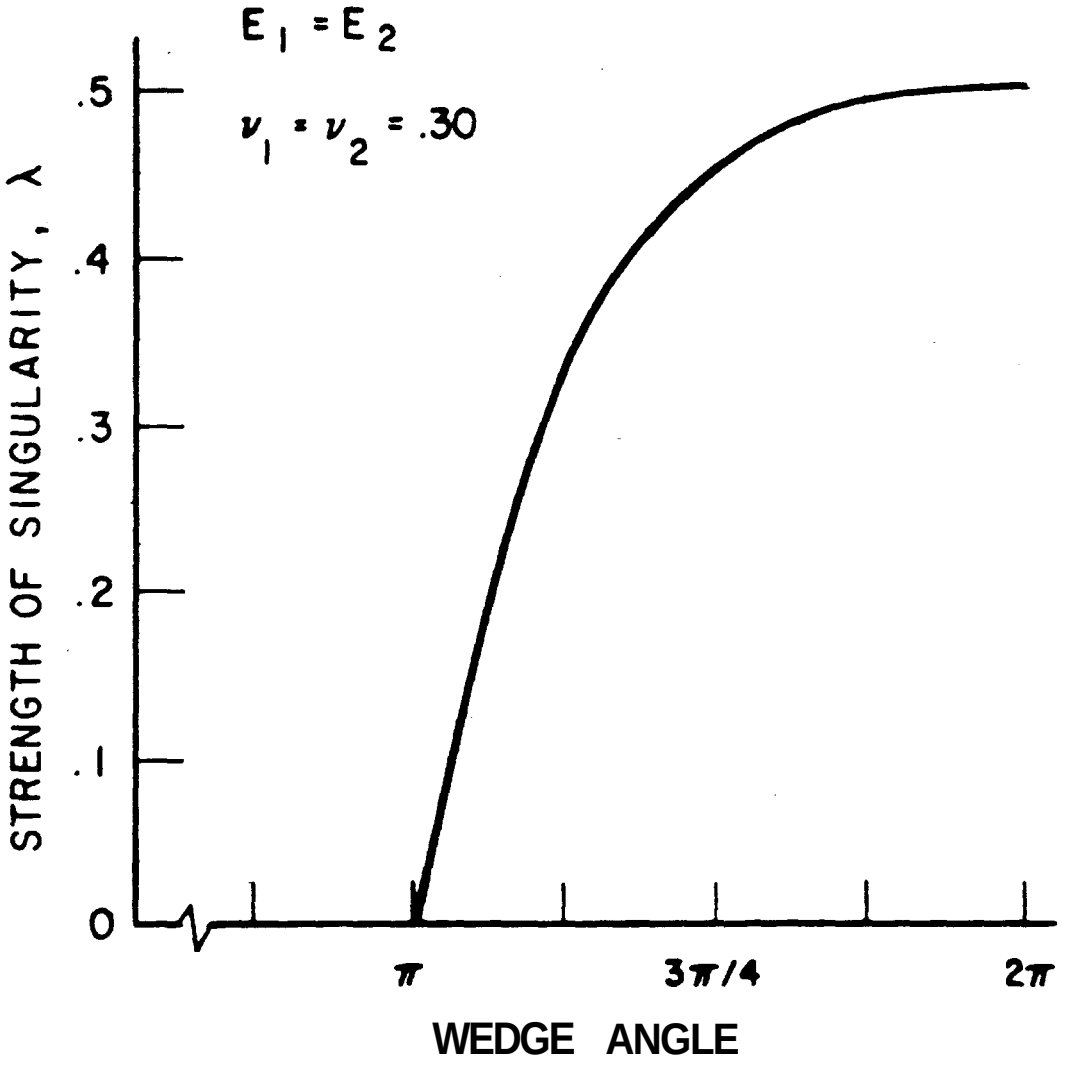

Fig. 3 **STRENGTH OF STRESS SINGULARITY** ($\sigma_{ij} \propto r^{-\lambda}$)

3. INTERACTION BETWEEN A CRACK AND A SOLID INCLUSION OR A PORE

In this section we will consider the problem of the interaction between a solid elastic inclusion and a line crack. It will be assumed that the inclusion and the crack are sufficiently close to each other so that their perturbed stress fields interact with each other. It will also be assumed that the crack-inclusion region is sufficiently far away from the boundaries so that their combined perturbed stress field does not interact with the boundaries, Consequently, for the purpose of calculating the perturbed stress state and the stress intensity factors it may be assumed that the domain is infinite.

3.1 Plane Strain Problem for a Circular Inclusion or Pore

Consider the general crack-inclusion problem described in Fig. 4. Assume that the composite medium is under plane strain or generalized plane stress conditions, with μ_i and κ_i, $(i=1,2)$ referring to the elastic constants (μ_i the shear modulus, $\kappa_i = 3-4\nu_i$ for plane strain, and $\kappa_i = (3-\nu_i)/(1+\nu_i)$ for plane stress, ν_i being the Poisson's ratio). Let u_t and u_w be the displacement components in t and w directions shown in Fig. 4(b). By defining

$$g_1(t) = \frac{\partial}{\partial t}(u_t^+ - u_t^-) \ , \ g_2(t) = \frac{\partial}{\partial t}(u_w^+ - u_w^-) \ , \tag{4}$$

and by referring to [10] for details, the problem may be formulated in terms of a pair of singular integral equations of the following form:

$$\frac{1}{\pi}\int_{t_2}^{t_1} \sum_{j=1}^{2} k_{ij}(t,t_o)g_j(t_o)dt_o = \frac{1+\kappa_1}{2\mu_1} p_i(t) \ , \ (i=1,2) \tag{5}$$

where the kernels k_{ij} are known functions and have a Cauchy type singularity. The known input functions p_1 and p_2 are given by

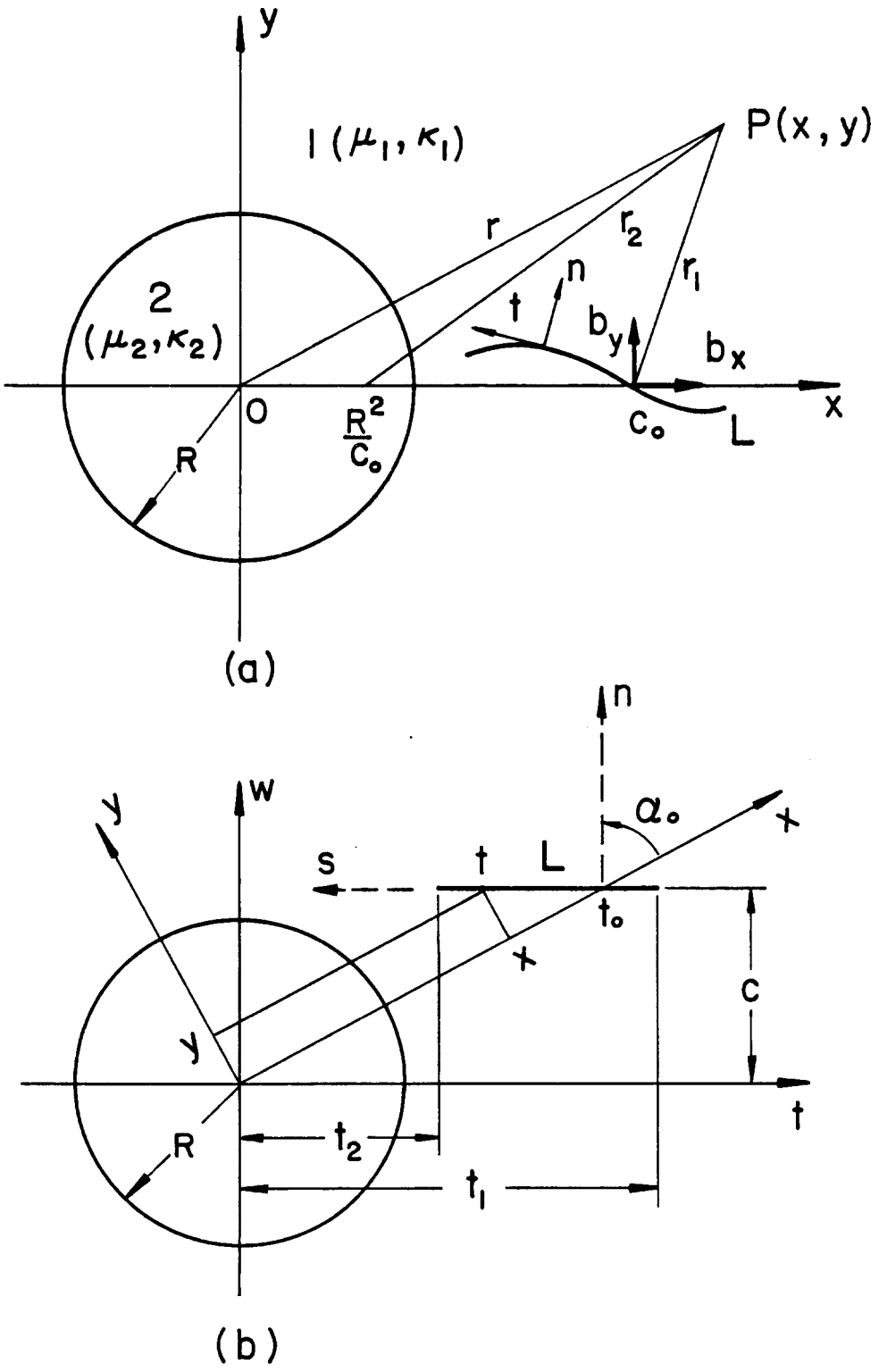

Figure 4. Geometry showing the dislocations b_x and b_y, and the crack L in the neighborhood of the inclusion 2.

$$p_1(t) = -\sigma_{ww}(t,c) \ , \ p_2(t) = -\sigma_{wt}(t,c) \ , \ (t_2<t<t_1) \ , \qquad (6)$$

σ_{ww} and σ_{wt} being the stress components at the point (t,c) in the plane with inclusion but without a crack. For example, for a plane under uniform tension σ_0 away from the inclusion these stresses are given by Fig. 2. The solution of (5) is of the following form

$$g_j(t) = G_j(t)/\sqrt{(t-t_2)(t_1-t)} \ , \ (j=1,2) \qquad (7)$$

where G_1 and G_2 are unknown bounded functions. After solving the integral equations the Modes I and II stress intensity factors at the crack tips t_1 and t_2 may be defined by and obtained from the following expressions:

$$k_1(t_1) = \lim_{t\to t_1} \sqrt{2(t-t_1)}\ \sigma_{ww}(t,c) = -\frac{2\mu_1}{1+\kappa_1} \lim_{t\to t_1} \sqrt{2(t_1-t)}\ g_2(t) \ ,$$

$$k_2(t_1) = \lim_{t\text{-}tt_1} \sqrt{t-t_1}\ \sigma_{wt}(t,c) = -\frac{2\mu_1}{1+\kappa_1} \lim_{t\to t_1} \sqrt{2(t_1-t)}\ g_1(t) \ ,$$

$$k_1(t_2) = \lim_{t\to t_2} \sqrt{2(t_2-t)}\ \sigma_{ww}(t,c) = \frac{2\mu_1}{1+\kappa_1} \lim_{t\ t_2} \sqrt{2(t-t_2)}\ g_2(t) \ ,$$

$$k_2(t_2) = \lim_{t\to t_2} \sqrt{2(t_2-t)}\ \sigma_{wt}(t,c) = \frac{2\mu_1}{1+\kappa_1} \lim_{t\to t_2} \sqrt{2(t-t_2)}\ g_1(t)$$

(8a-d)

In the absence of a crack the stress components on a line perpendicular to the loading direction are shown in Fig. 2 for an elastic inclusion. Similar results for a circular hole (i.e., for $\mu_2=0$) are shown in Fig. 5.

The stress intensity factors calculated at the crack tips t_1 and t_2 are shown in Figures 6-13. The results shown in the figures are normalized with respect to $\sigma_0\sqrt{a}$ where σ_0 is the tensile stress acting on the plane away from and perpendicular to the crack and a is the half crack length. Thus, the normalized stress intensity factors k_{ij} shown in the

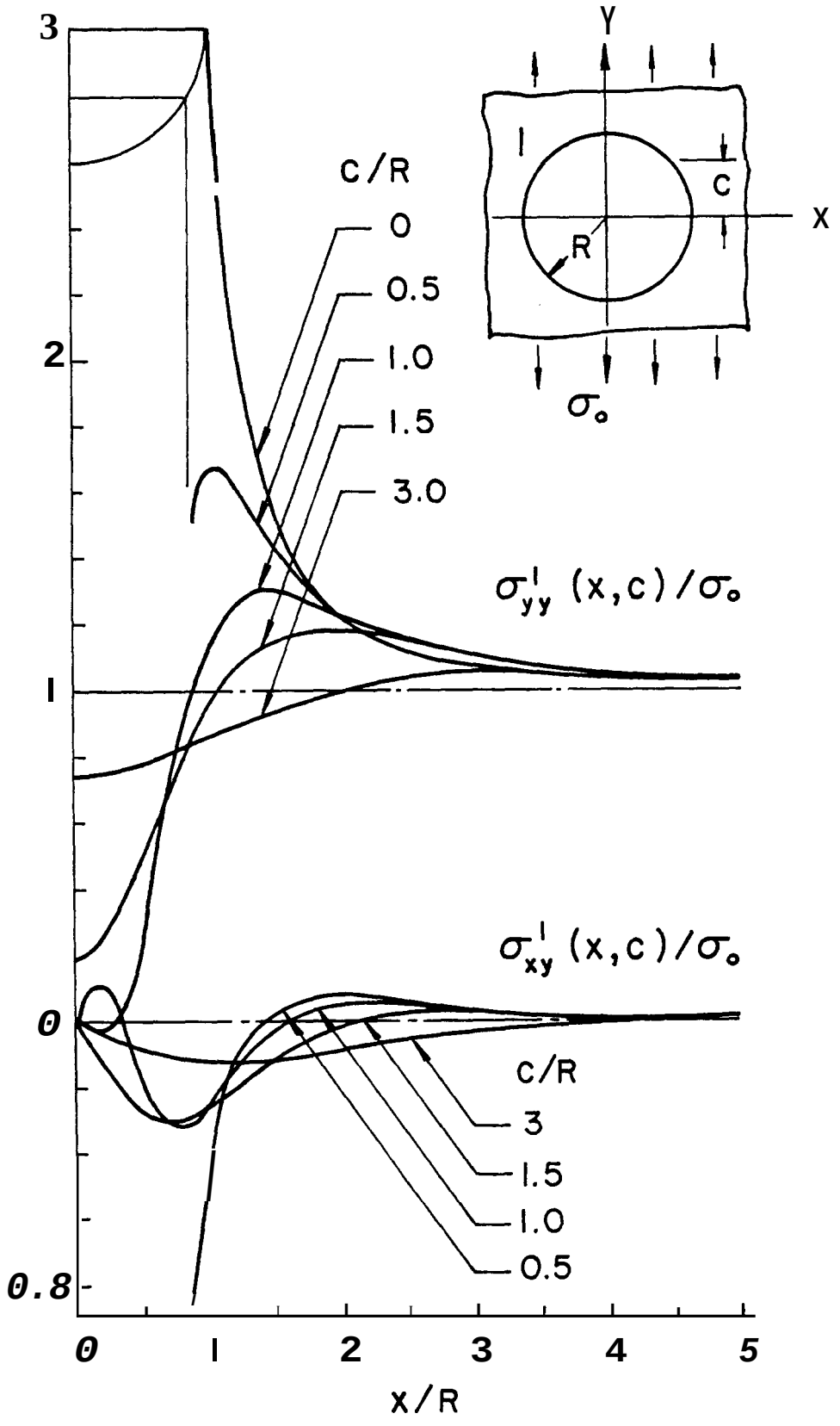

Figure 5. The stress distribution in a plate with a circular hole.

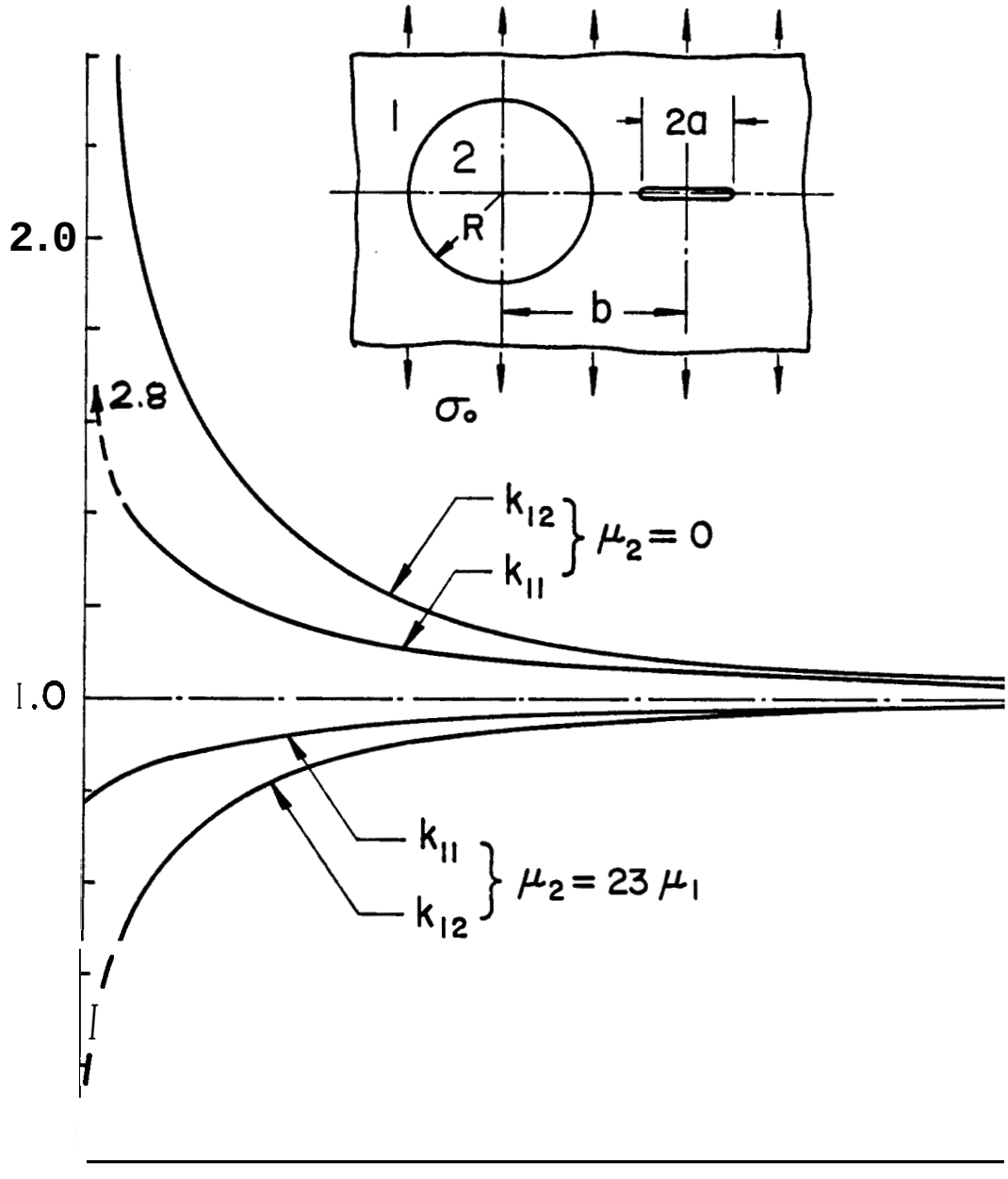

Figure 6. The stress intensity factors for a symmetrically located radial crack (R/a = 2, C = 0).

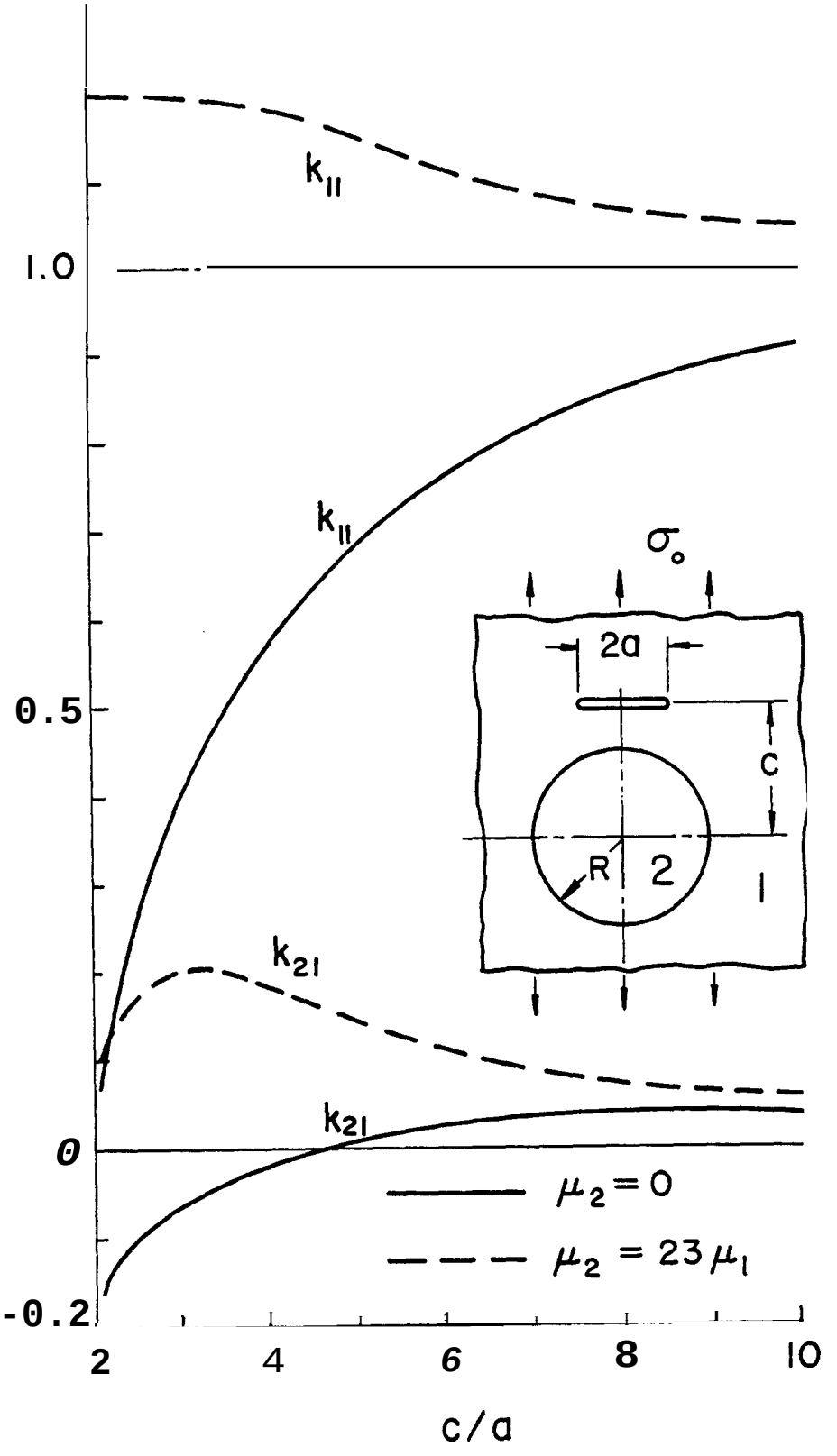

Figure 7. The stress intensity factors for a symmetrically located "tangential crack" perpendicular to the load (b = 0, R = 2a).

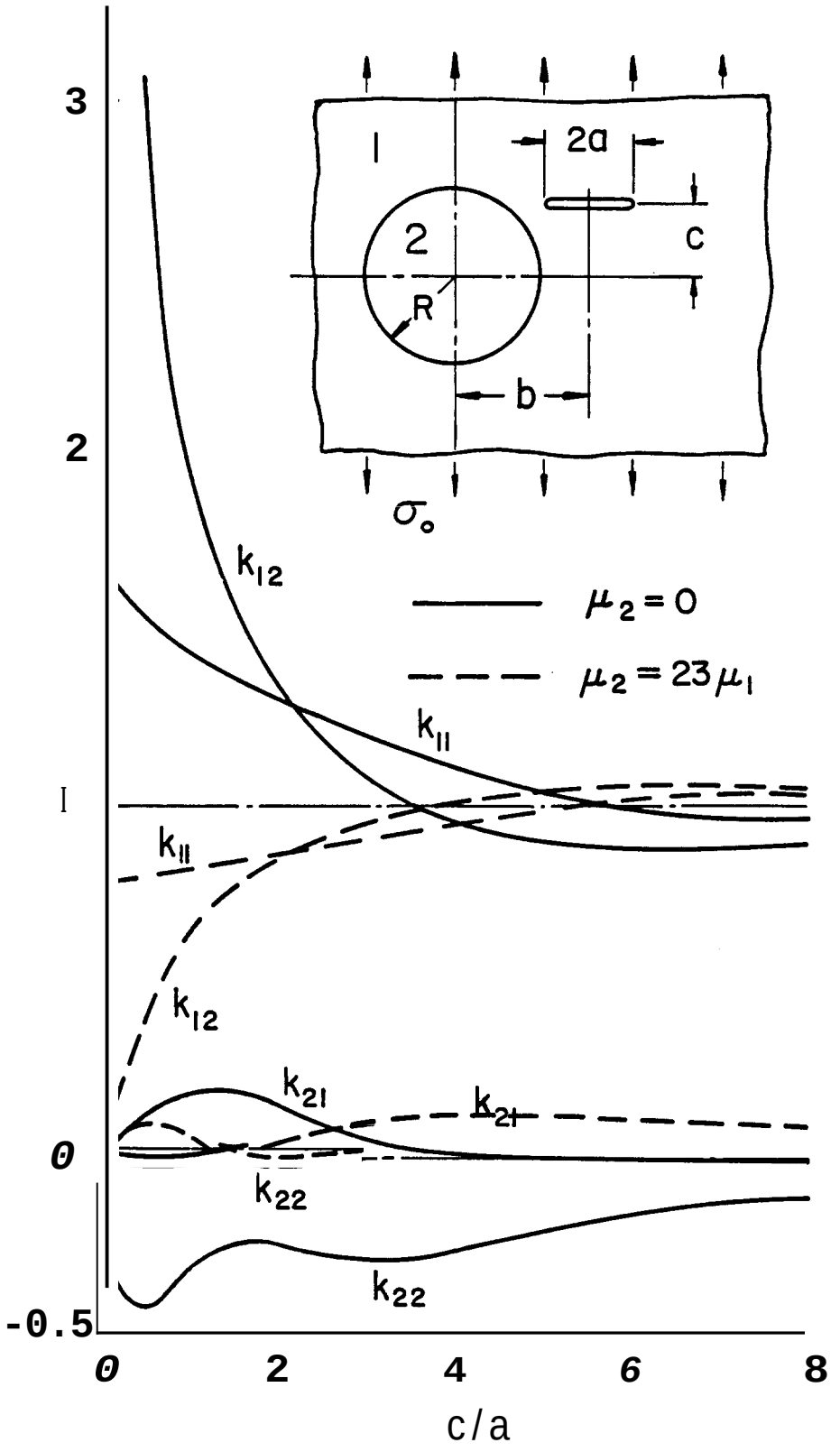

Figure 8. Stress intensity factors for a crack perpendicular to the external load (R = 2a, b = 3a).

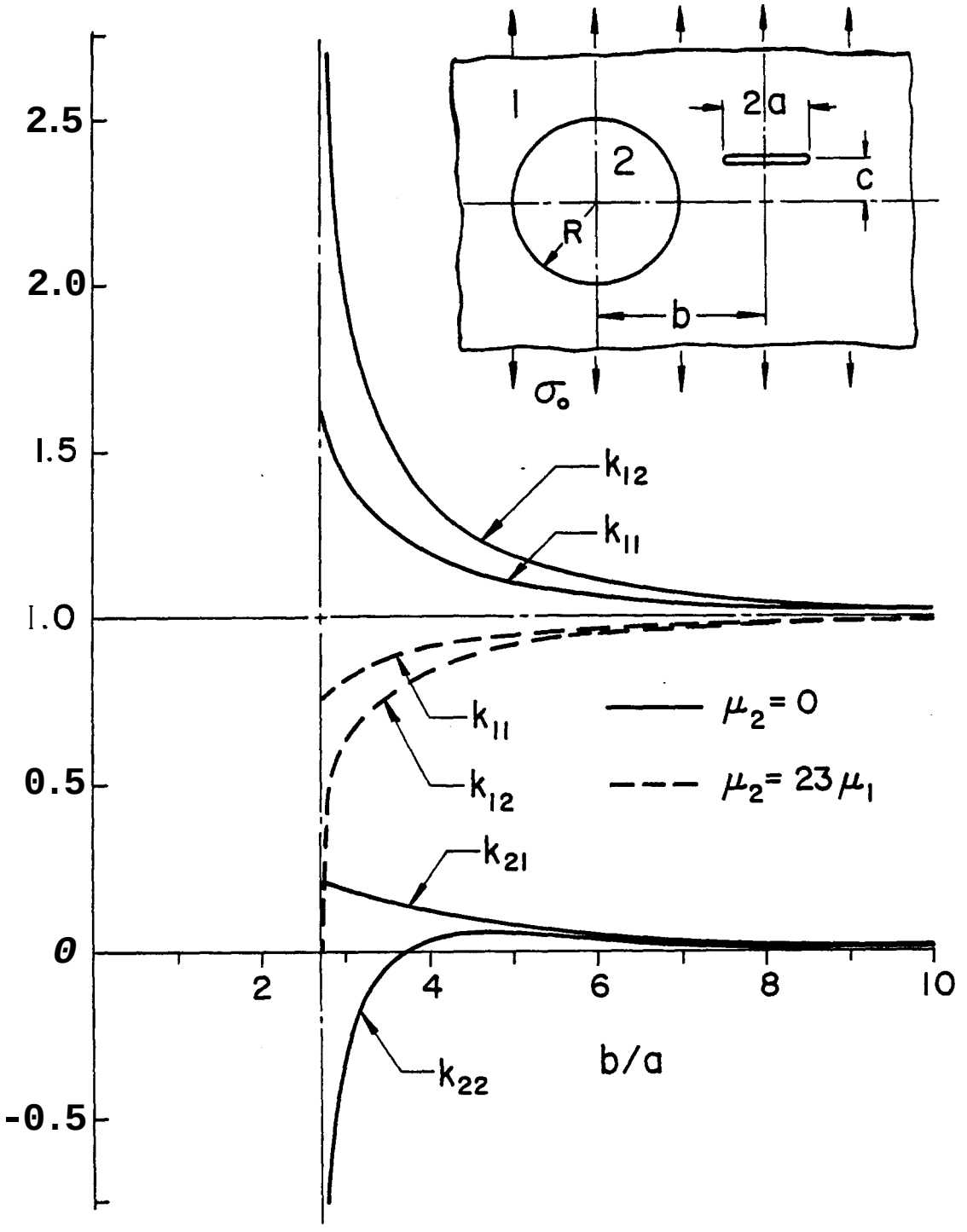

Figure 9. Stress intensity factors for a crack perpendicular to the external load (R = 2a, c = a).

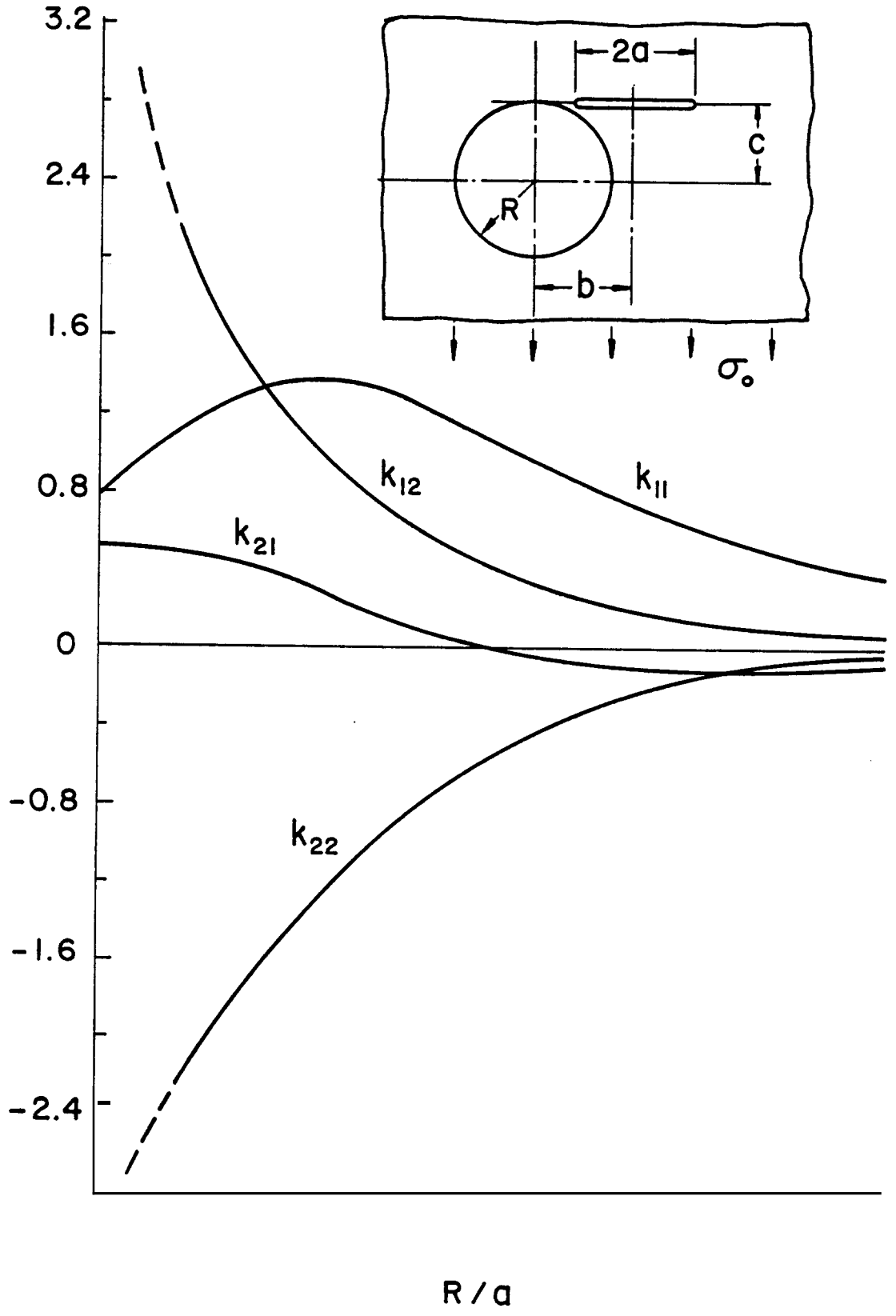

Figure 10. Stress intensity factors for a crack in the matrix containing a circular hole ($\mu_2 = 0$, c = R, b-a = 0.2R, a = constant).

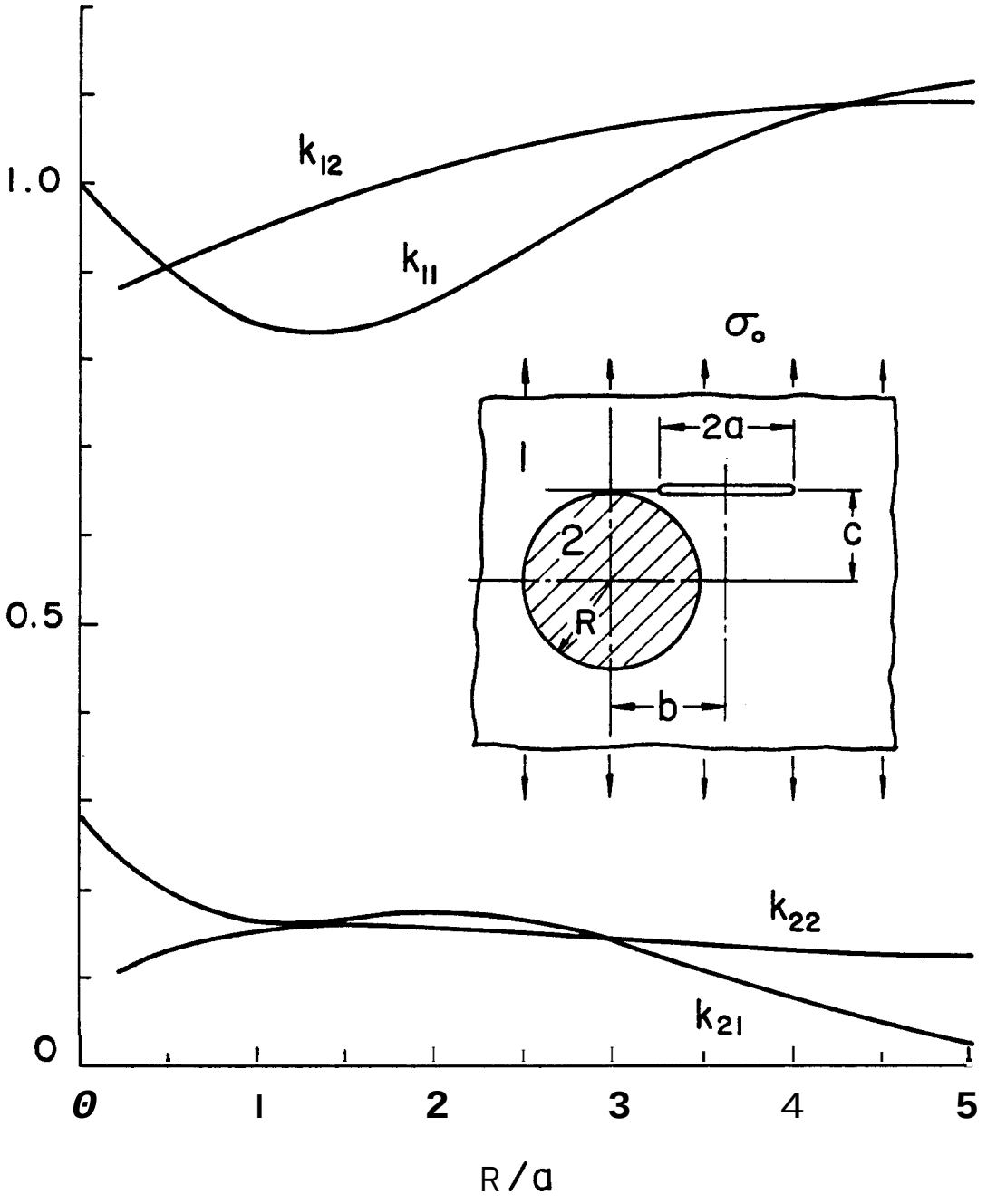

Figure 11. Stress intensity factors for a crack in the matrix containing an elastic inclusion ($\mu_2 = 23\mu_1$, c = R, b-a = 0.2R, a = constant).

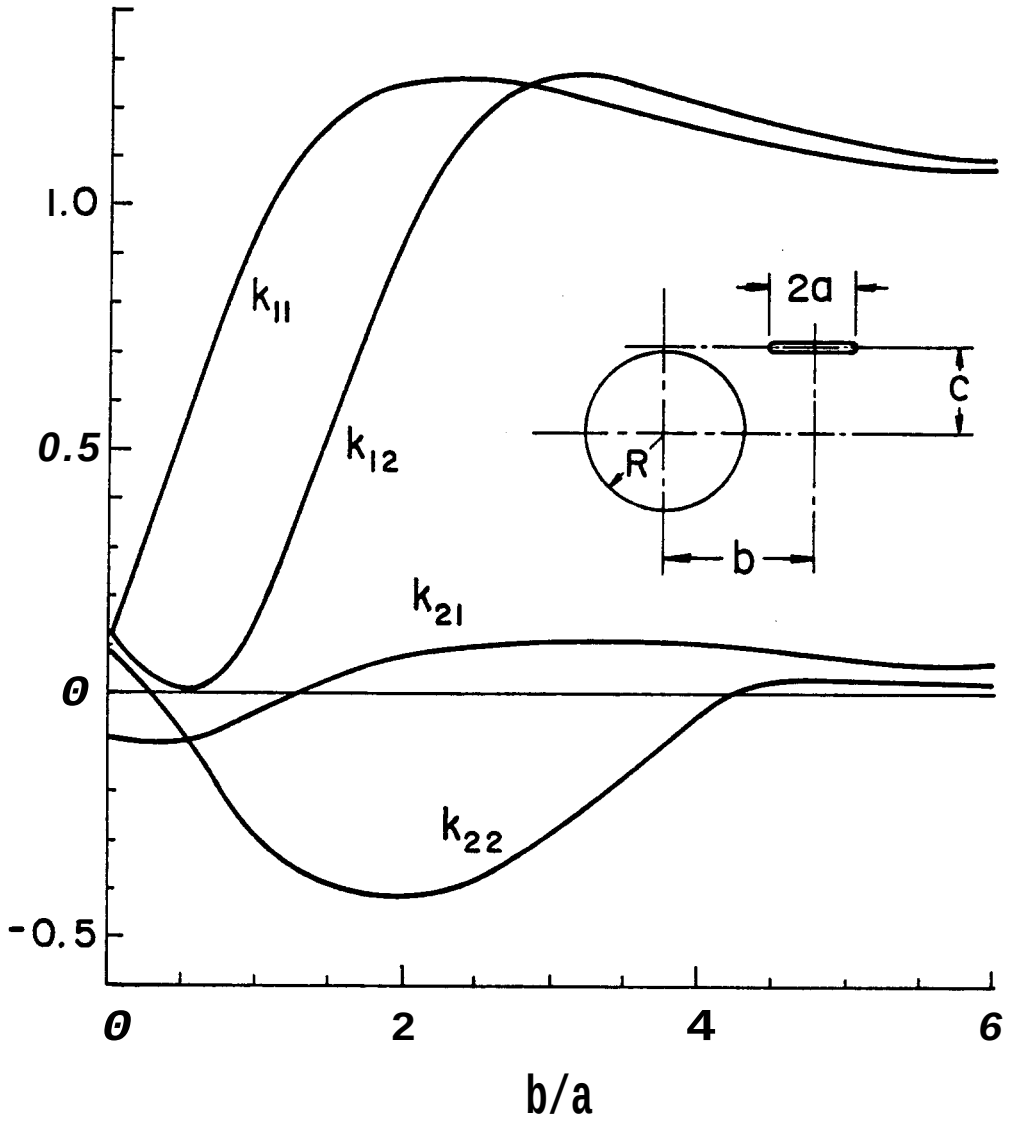

Figure 12. Stress intensity factors for a crack in the matrix containing a circular hole ($\mu_2 = 0$, $c = 2.2a$, $R = 2a$).

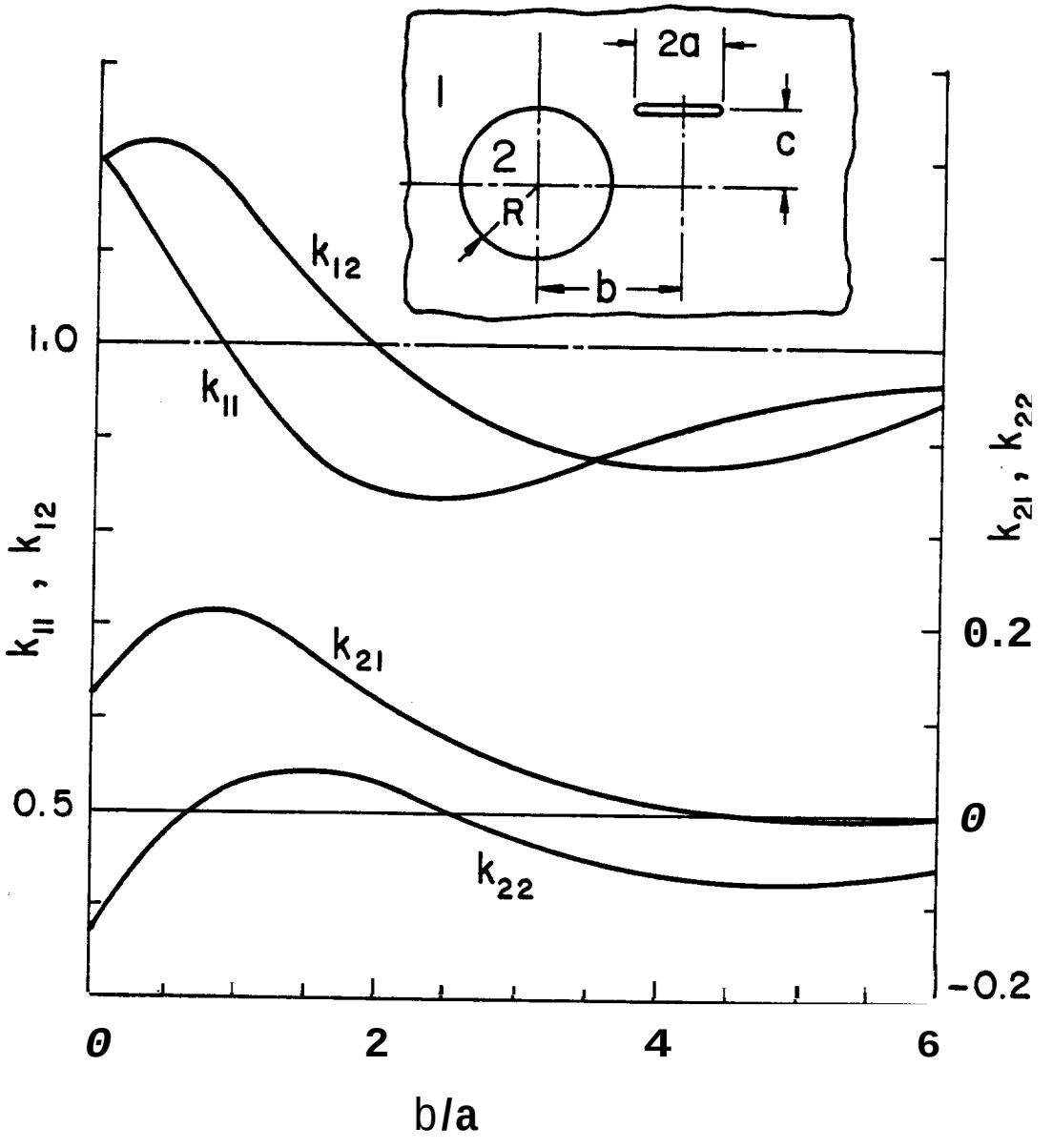

Figure 13. Stress intensity factors for a crack in the matrix containing an elastic inclusion ($\mu_2 = 23\mu_1$, $c = 2.2a$, $R = 2a$).

figures are defined by

$$k_{ij} = \frac{k_i(t_j)}{\sigma_0\sqrt{a}} \quad , \quad (i,j = 1,2) \tag{9}$$

where $k_i(t_j)$ are given in (8). Figures show the results for only two cases, namely a circular hole (i.e., $\mu_2=0$) and a stiffer elastic inclusion with elastic constants

$$(\mu_2/\mu_1) = 23 \quad , \quad \kappa_1 = 1.6 \ , \ \kappa_2 = 1.8 \quad . \tag{10}$$

Fig. 6 shows the results for a symmetrically located radial crack. Note that as the (inner) crack tip t_2 approaches the boundary (i.e., for $b \to R+a$) the stress intensity factor $k_1(t_2)$ tends to infinity for the case of hole and to zero for the case of inclusion. Qualitatively the results given in this figure are very general, that is if the perturbed stress fields of a crack and a hole (or a pore) interact, then the stress intensity factors at the crack tips would be greater than those which would be obtained for the cracked medium without the hole. For example, note that in Fig. 6 the stress intensity factors for $\mu_2=0$ are greater than $\sigma_0\sqrt{a}$, the value for the cracked plane without a hole, and approach this value as the crack moves away from the hole (i.e., as $b \to \infty$). Similar trend would be observed for an inclusion the stiffness of which is less than that of the cracked medium (i.e., for $\mu_2<\mu_1$). On the other hand, if the plane contains a stiffer inclusion (i.e., for $\mu_2>\mu_1$), then the stress intensity factors are smaller than $\sigma_0\sqrt{a}$.

The results shown in Figures 7-13 are self-explanatory. Depending on the location of the crack, one may observe some trends in these results which are opposite to that observed for the symmetric radial crack shown in Fig. 6. These trends, however, may easily be explained by examining the stress fields perturbed by an inclusion or a hole which are shown in figures 2 and 5. By examining the signs of the Modes I and II stress intensity factors, from the results given in these figures one may easily conclude that generally for the crack tip near the matrix-inclusion boundary the crack would propagate towards the boundary if

$\mu_2=0$ or $\mu_2<\mu_1$, and away from the boundary if $\mu_2>\mu_1$. This conclusion is based on the analysis giving the plane of the maximum cleavage stress at the crack tip. The details of the analysis and its experimental verification may be found in [12].

In another class of crack-inclusion interaction problems both the inclusion and the matrix material may contain a crack. For symmetrically located radial cracks the general problem is described by Fig. 14. The details of the analysis of this problem may be found in [11]. Figures 15-21 show some calculated results. In this problem the formulation given in [11] and Fig, 14 allow the consideration of the special cases of a crack terminating at the interface (i.e., $b=R+a$, $\mu_2\neq 0$ in Fig. 6 or $a_2=b_2$, $a_1=a$ in Fig. 14), and the crack going through the interface (i.e., $b_2=a=a_1$ in Fig, 14). In these special cases it is shown that [11] the point ($x=a$, $y=0$) (Fig. 14) is a point of stress singularity and the stress state in a close neighborhood of it has the following form:

$$\sigma_{ij}(r,\theta) = \frac{k}{r^{\beta}} g_{ij}(\theta) \quad , \quad (i,j=x,y) \quad , \quad (0<\beta<1) \tag{11}$$

where r and θ are the polar coordinates centered at the singular point, g_{ij} is a bounded function and the stress intensity factor k is a constant. The stress intensity factors $k = k(a)$ given in this section are defined in terms of the related cleavage stresses as follows (Fig. 14):

(i) crack in the matrix ($-a<a_2<b_2<a = a_1<b_1$):

$$k(a) = \lim_{x\to a} \sqrt{2}\,(a-x)^{\beta}\sigma_{2yy}(x,0) \quad , \tag{12}$$

(ii) crack in the inclusion ($-a<a_2<b_2 = a<a1<b1$):

$$k(a) = \lim_{x\to a} \sqrt{2}\,(x-a)^{\alpha}\sigma_{1yy}(x,0) \tag{13}$$

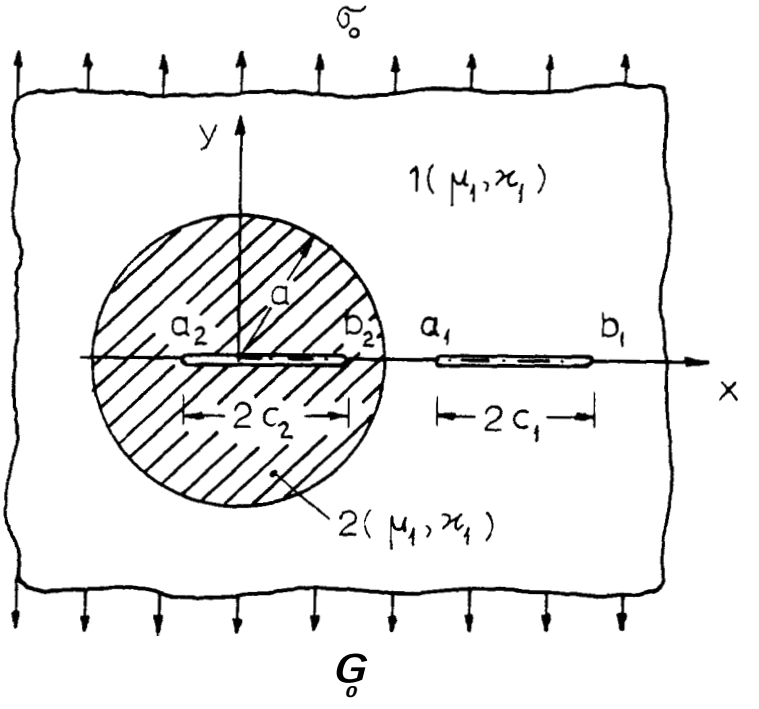

Figure 14. **Inclusion-crack** geometry.

(iii) crack crossing the boundary ($-a<a_2<b_2 = a = a_1<b_1$):

In this case for simplicity we define the following normal and shear cleavage stress intensity factors

$$k_{xx}(a) = \lim_{y\to 0} y^{\gamma}\, \sigma_{1xx}(a,y) \quad \text{, (normal cleavage)} \quad , \tag{14}$$

$$k_{xy}(a) = \lim_{y\to 0} y^{\gamma}\, \sigma_{1xy}(a,y) \quad \text{, (shear cleavage)} \quad . \tag{15}$$

The first special problem (i) with $a_2=b_2$ corresponds to the limiting case of the problem considered in Fig, 6. In the problem of a crack terminating at the bimaterial interface such as the cases (i) and (ii) mentioned above, the power of the stress singularity (α or β) is highly dependent on the stiffness ratio μ_2/μ_1 and is relatively insensitive to the Poisson's ratios (or κ_1 and κ_2). For the crack geometry $a_2=b_2$, $a_1=a$, $b_1>a$, Fig. 14, Table 1 shows the effect of μ_2/μ_1 on β. It may be seen that for $(\mu_2/\mu_1)<1$ the power β is greater than 0.5, meaning that if the stiffness of the inclusion is less than that of the matrix, then the stress singularity is stronger than the corresponding homogeneous case. Similarly, if $\mu_2>\mu_1$ then $\beta<0.5$. This is the reason for the asymptotic trends observed in Fig. 6 for the stress intensity factor $k(a)$ as $b\to R+a$. Table 1 also gives the corresponding stress intensity factors calculated from (12).

For this problem, to give some idea about the nature and the relative magnitude of the crack surface displacement, Fig. 15 shows some calculated results. Here $v(x,0)$ is the crack surface displacement in y direction.

Figures 16 and 17 show the stress intensity factors for a crack located in the inclusion. The limiting values of the stress intensity factors shown in these figures for the crack length $2c_2$ approaching zero are obtained from uniformly loaded "infinite" plane solution with the applied stress state away from the crack region given by the uncracked

Table 1. The effect of modulus ratio on the stress intensity factors for a crack terminating at the interface ($a_1 = a$, $b_1/a = 2$, $\kappa_1 = \kappa_2 = 1.8$, $c_1 = (b_1 - a)/2$).

$m = \frac{\mu_2}{\mu_1}$	β	$\frac{k(b_1)}{\sigma_0\sqrt{c_1}}$	$\frac{k(a)}{\sigma_0 c_1^{\beta}}$
0		2.808	
0.05	0.81730	1.615	1.053
1/3	0.62049	1.229	0.5836
1.0	0.5	1.000	1.000
3.0	0.40074	0.8610	1.299
10.0	0.33277	0.7969	1.389
23.0	0.30959	0.7796	1.375
100	0.29387	0.7691	1.345
300	0.28883	0.7667	1.348

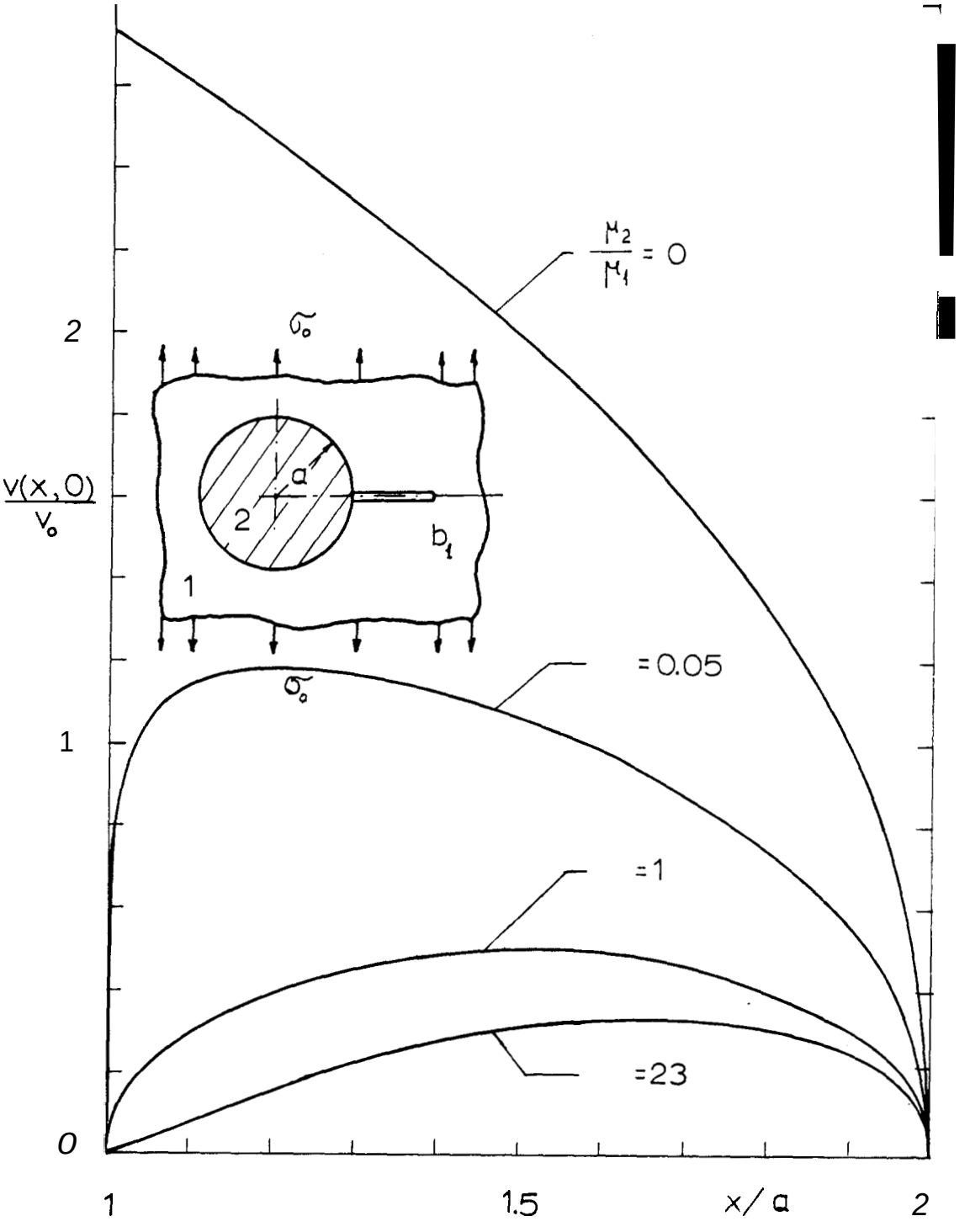

Figure 15. Crack surface displacement for a crack in the matrix with one tip on the interface ($\kappa_1 = \kappa_2 = 1.8$, $b_1/a = 2$, $v_o = (1+\kappa_1)a\sigma_o/\mu_1$).

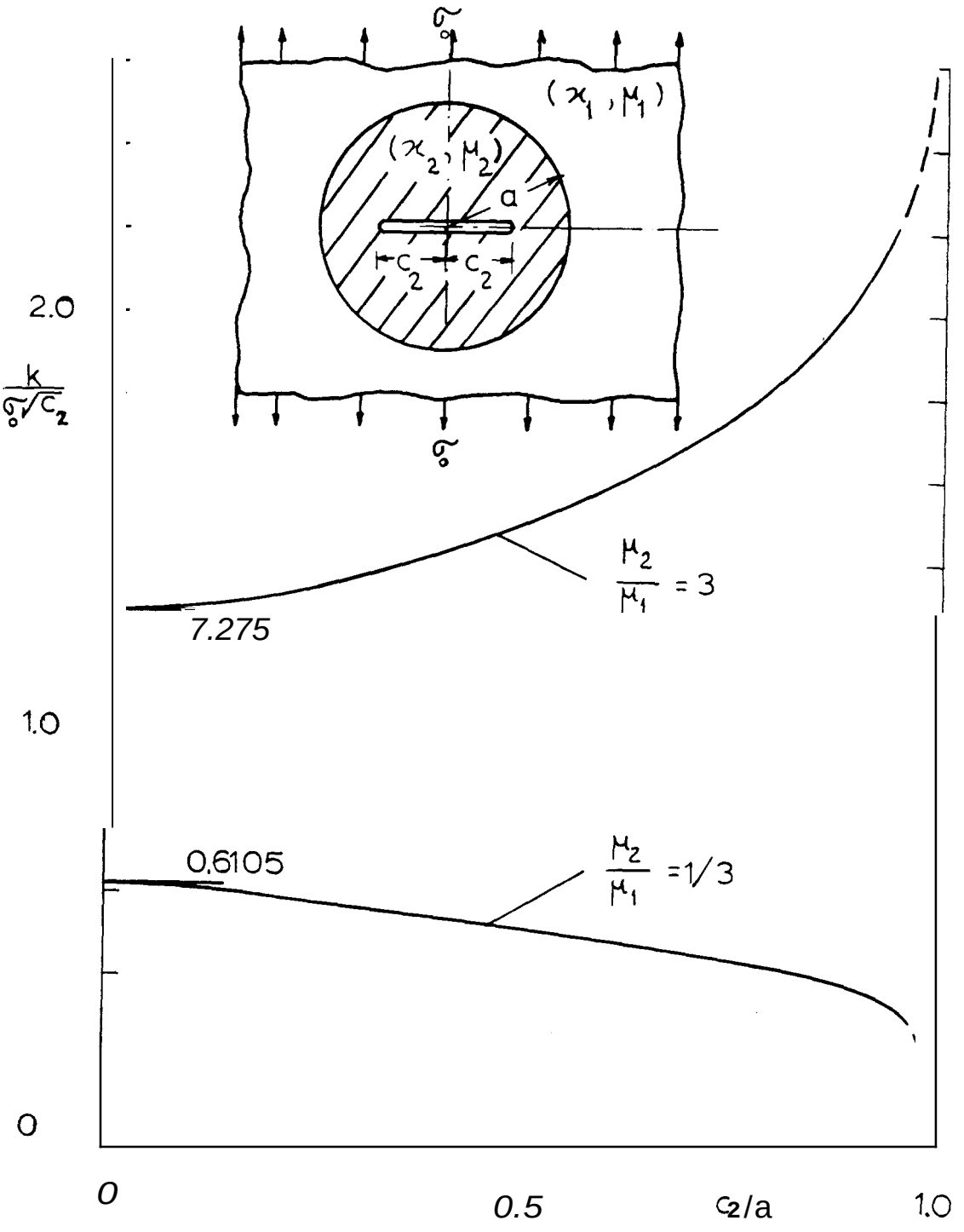

Figure 16. Stress intensity factor for a symmetrically located crack in the inclusion ($\kappa_1 = \kappa_2 = 1.8$).

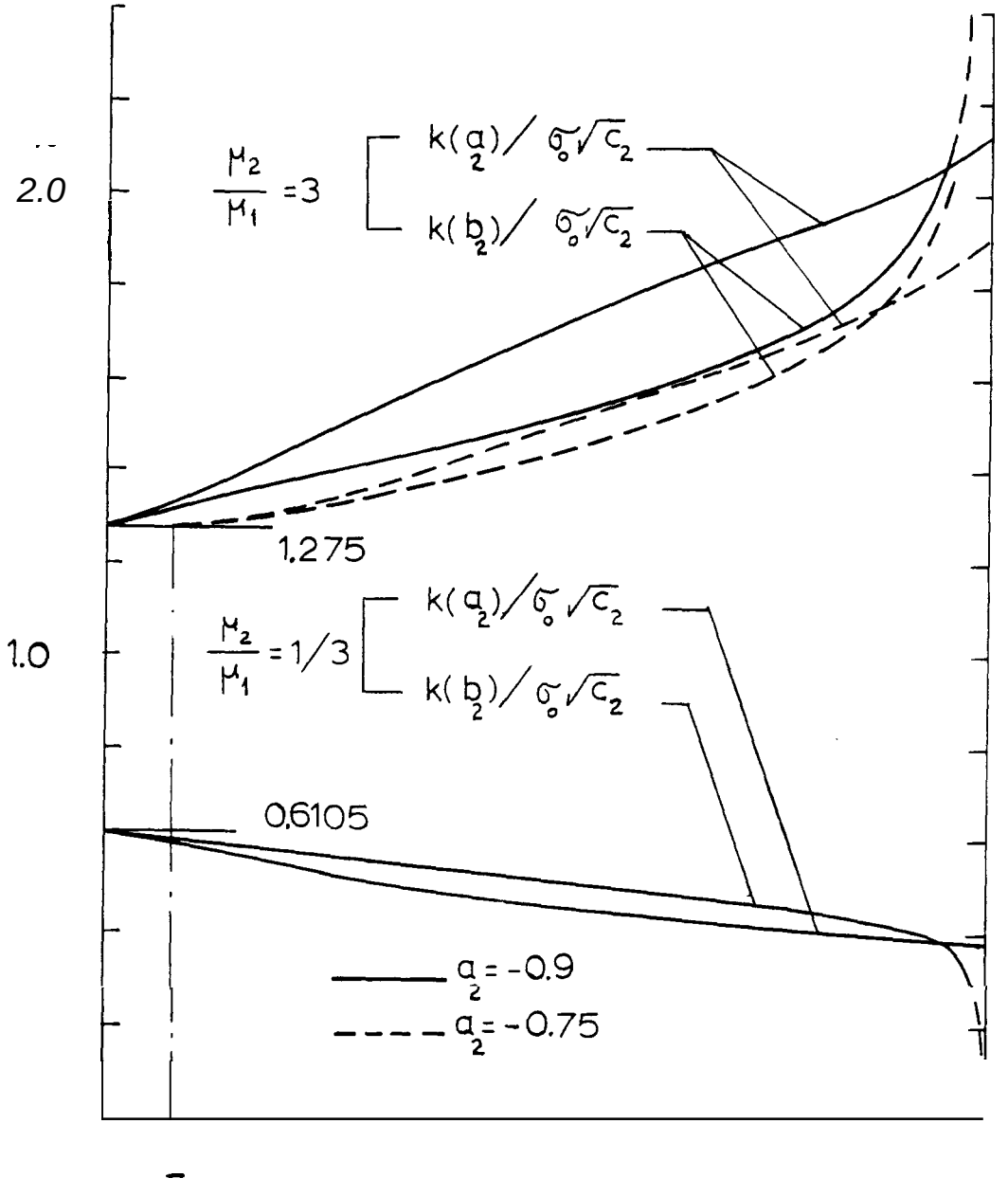

Figure 17. Stress intensity factors for a crack located in the inclusion ($\kappa_1=\kappa_2=1.8$, one tip fixed at $a_2=-0.9a$ or $a_2=-0.75a$, b_2 variable, $c_2=(b_2-a_2)/2$).

inclusion solution [13], namely

$$\sigma^{a}_{2yy}(x,0) = \sigma_o \frac{(1+\kappa_1)\mu_2}{2\mu_1}\left(\frac{1}{\kappa_2-1+2\mu_2/\mu_1} + \frac{1}{1+\kappa_1\mu_2/\mu_1}\right), \quad |x|<a, \tag{16}$$

$$\sigma^{a}_{1yy}(x,0) = \sigma_o\left[1 - \frac{a^2}{2x^2}\frac{\mu_2(\kappa_1-1)-\mu_1(\kappa_2-1)}{2\mu_2+\mu_1(\kappa_2-1)} - \frac{a^4}{x^4}\frac{3(\mu_2-\mu_1)}{2(\mu_1+\kappa_1\mu_2)}\right], \quad |x|>a, \tag{17}$$

$$\sigma^{a}_{1xy}(x,0) = 0, \quad \sigma^{a}_{2xy}(x,0) = 0. \tag{18}$$

By using (16) it may be shown that for the crack in the inclusion the stress intensity factor has the following limit:

$$\lim_{c_2\to 0} \frac{k}{\sigma_o\sqrt{c_2}} = \frac{\mu_2(\kappa_1+1)}{2\mu_1}\left(\frac{\mu_1}{2\mu_2+\mu_1(\kappa_2-1)} + \frac{\mu_1}{\mu_1+\kappa_1\mu_2}\right). \tag{19}$$

Fig. 16 shows the results for a symmetrically located crack. The results for an eccentric crack are shown in Fig. 17 (see Fig. 14 for notation).

Some typical results for the case in which both the inclusion and the matrix or base material contain a crack are shown in Fig. 18.

The stress intensity factor for a completely cracked inclusion (i.e., for $a_2=-a$, $b_2=a$, $a_1=b_1$) is given in Table 2. The stress intensity factor $k(a)$ given in this table is defined by (13) where α is the power of stress singularity.

The stress intensity factors for a crack crossing the interface are given by figures 19 and 20. In these figures $x=a_2$ and $x=b_1$ are conventional crack tips for which the stress state has square-root singularity (i.e., $\alpha'=\beta'=0.5$). For the point of the intersection of the crack with the boundary ($x=a$) the normal and shear cleavage components of the stress intensity factor k_{xx} and k_{xy} are defined by (14) and (15). The asymptotic trends of the stress intensity factors observed in these figures as a crack tip approaches the boundary $x=a$ are again due to the change in the

Table 2. Stress intensity factor for a completely cracked inclusion.

$\frac{\mu_2}{\mu_1}$	$\kappa_1 = \kappa_2 = 1.8$		$\kappa_1 = 2.2$, $\kappa_2 = 1.8$		$\kappa_1 = 1.8$, $\kappa_2 = 2.2$		$\kappa_1 = \kappa_2 = 2.2$	
	α	$\frac{k(a)}{\sigma_0 a^{\alpha}}$	α	$\frac{k(a)}{\sigma_0 a^{\alpha}}$	α	$\frac{k(a)}{\sigma_0 a^{\alpha}}$	a	$\frac{k(a)}{a}$
0.2	3.36621	0.7890	0.38087	0.7848	0.32027	1.046	0.33845	1.010
0.6	3.45025	1.014	0.47028	0.9456	0.42123	1.174	0.44466	1.068
1.0	3.5	1.0	0.51991	0.9209	0.47724	1.107	0.5	1.0
2.0	3.57451	0.8843	0.59188	0.8165	0.55687	0.9465	0.57624	0.8613
5.0	3.67885	0.6555	0.69124	0.6194	0.66380	0.6940	0.67733	0.6500

power of stress singularity. For example, in Fig. 19 for $b_1>a$ the stress components around the singular point $(x=a, y=0)$ are (see (14) and (15))

$$\sigma_{xx}(a,y) \cong \frac{k_{xx}(a)}{y^{\gamma}} \quad , \quad \sigma_{xy}(a,y) \cong \frac{k_{xy}(a)}{y^{\gamma}} \quad , \quad \gamma = 0.27326. \tag{20}$$

On the other hand, for $b_1=a$ (i.e., the case of a crack in the inclusion terminating at the boundary) the stress state around $(x=a, y=0)$ is given by (see eq. (13))

$$\sigma_{ij} = \frac{k(a)}{\sqrt{2}\, r^{\alpha}} f_{ij}(\theta) \quad , \quad \alpha = 0.82580 \ , \tag{21}$$

where r and θ are the polar coordinates centered at the point $(x=a, y=0)$ (i.e., $r=y$ for $\theta = \pi/2$). Thus, as $b_1 \to a$ from (20) and (21) it follows that

$$\sigma_{xx}(a,y) \cong \frac{k_{xx}(a)}{y^{\gamma}} + \frac{k(a)}{\sqrt{2}\, y^{\alpha}} f_{xx}\left(\frac{\pi}{2}\right) \tag{22}$$

or

$$\sigma_{xx}(a,y) \to \frac{1}{y^{\gamma}} \left[\frac{k(a)}{\sqrt{2}\, y^{\alpha-\gamma}} f_{xx}(\pi/2) \right] , \tag{23}$$

and

$$k_{xx}(a) \to \frac{k(a)}{\sqrt{2}\, y^{\alpha-\gamma}} f_{xx}(\pi/2) \quad . \tag{24}$$

Since $k(a)$ and f_{xx} are bounded and $\alpha>\gamma$, for $y=0$ (at which, by (14), k_{xx} must be calculated) $k_{xx}(a)$ would become unbounded. Similarly, it is seen that for $b_1 \to a$, k_{xy} tends to (negative) infinity. Also, since α (for the terminating crack tip) is greater than 0.5 (at b_1 for the embedded crack tip), by following a similar argument it may be shown that as $b_1 \to a$, $k(b_1)$ becomes unbounded.

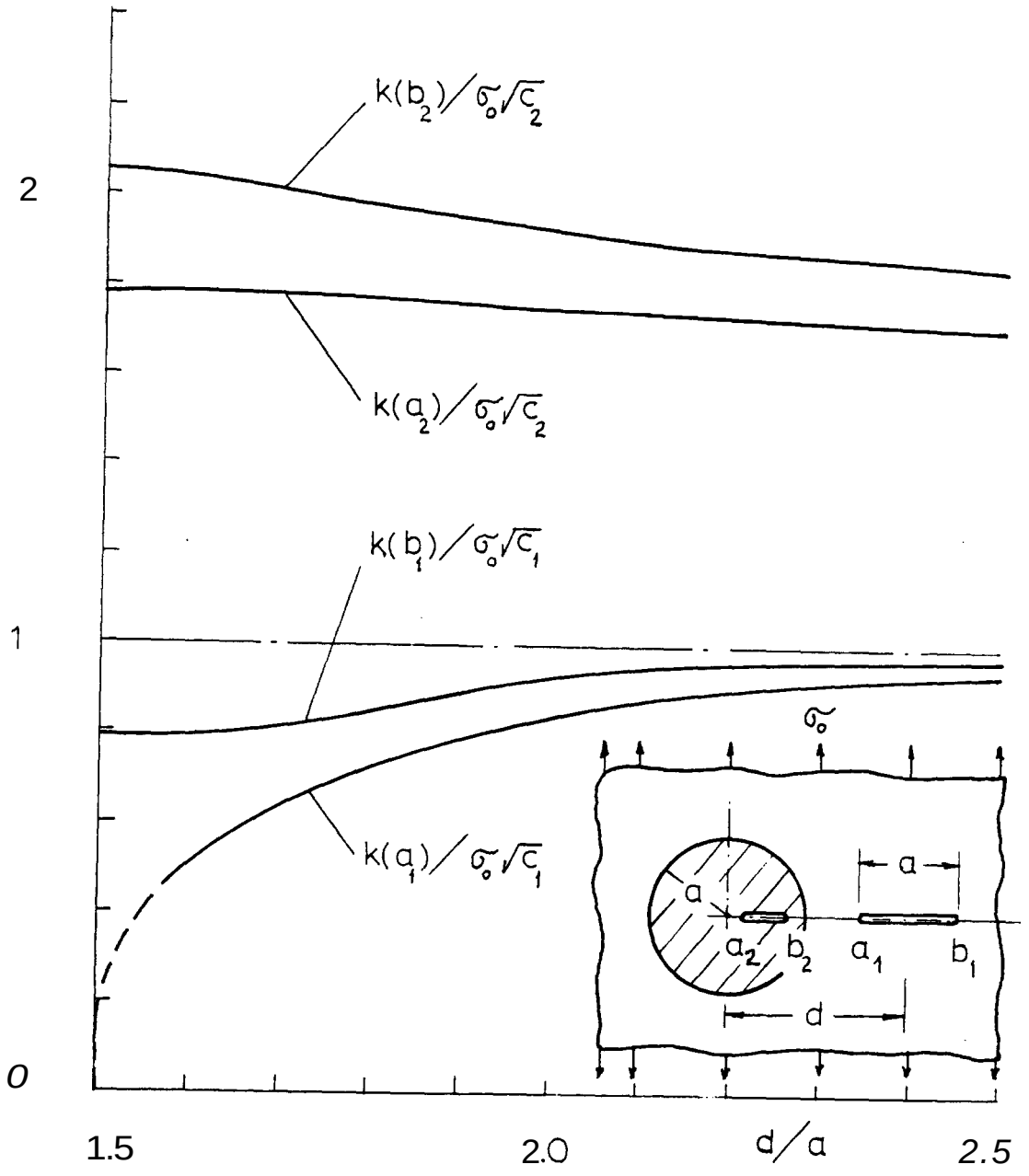

Figure 18. Stress intensity factors for a crack in the matrix (epoxy) and a crack in the inclusion (aluminum) ($\kappa_1 = 1.6$, $\kappa_2 = 1.8$, $\mu_2/\mu_1 = 23.077$; $a_2 = 0.3a$, $b_2 = 0.8a$, $2c_1 = (b_1 - a_1) = a$ fixed, $d = (b_1 + a_1)/2$ variable).

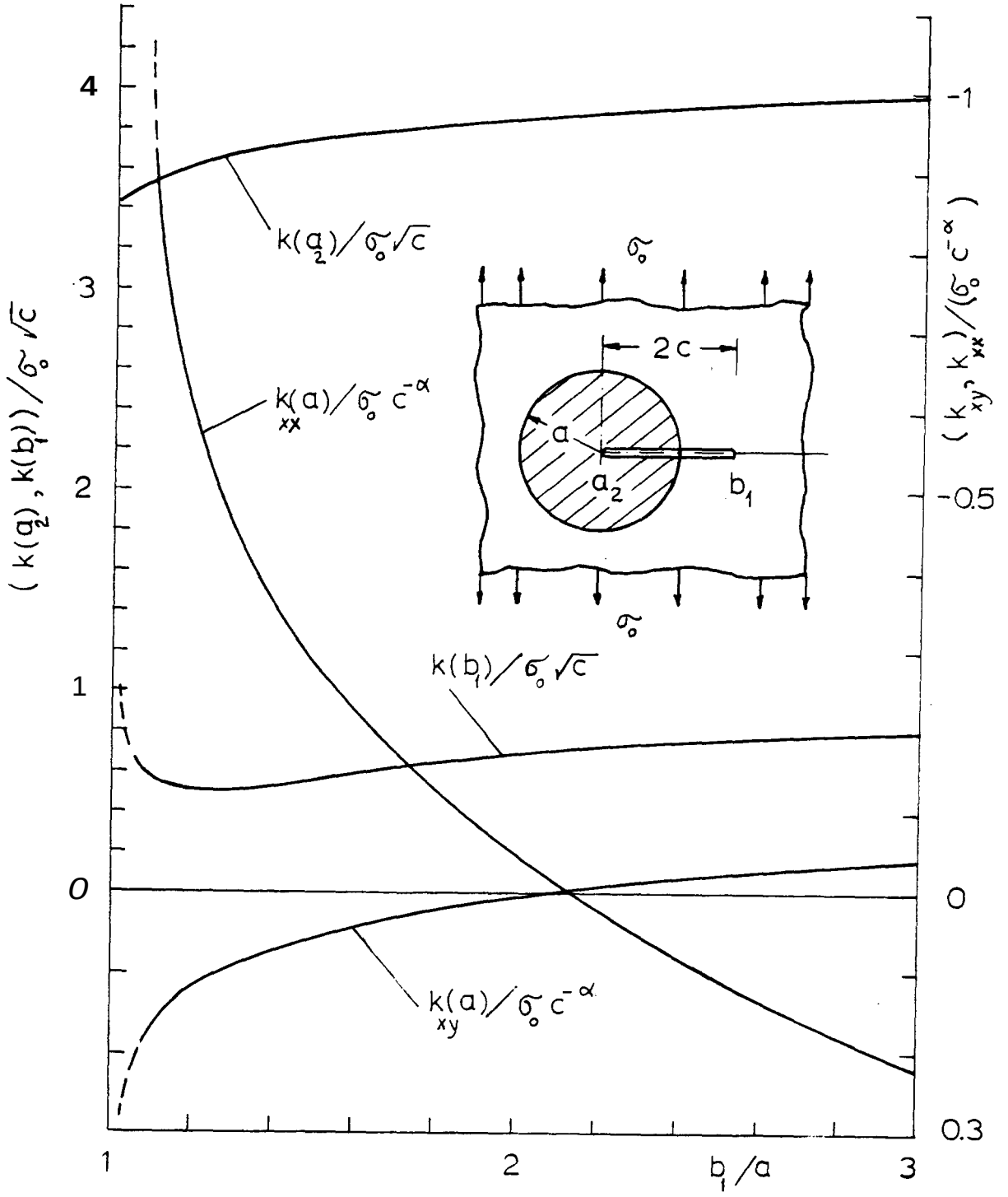

Figure 19. Stress intensity factors for a crack going through the matrix-inclusion interface ($\kappa_1 = 1.6$, $\kappa_2 = 1.8$, $\mu_2/\mu_1 = 23.077$, $\alpha' = \beta' = -0.5$, $\gamma = \alpha = \beta = 0.27326$, $c = (b_1 - a_2)/2$, $a_2 = 0$ fixed, b_1 variable).

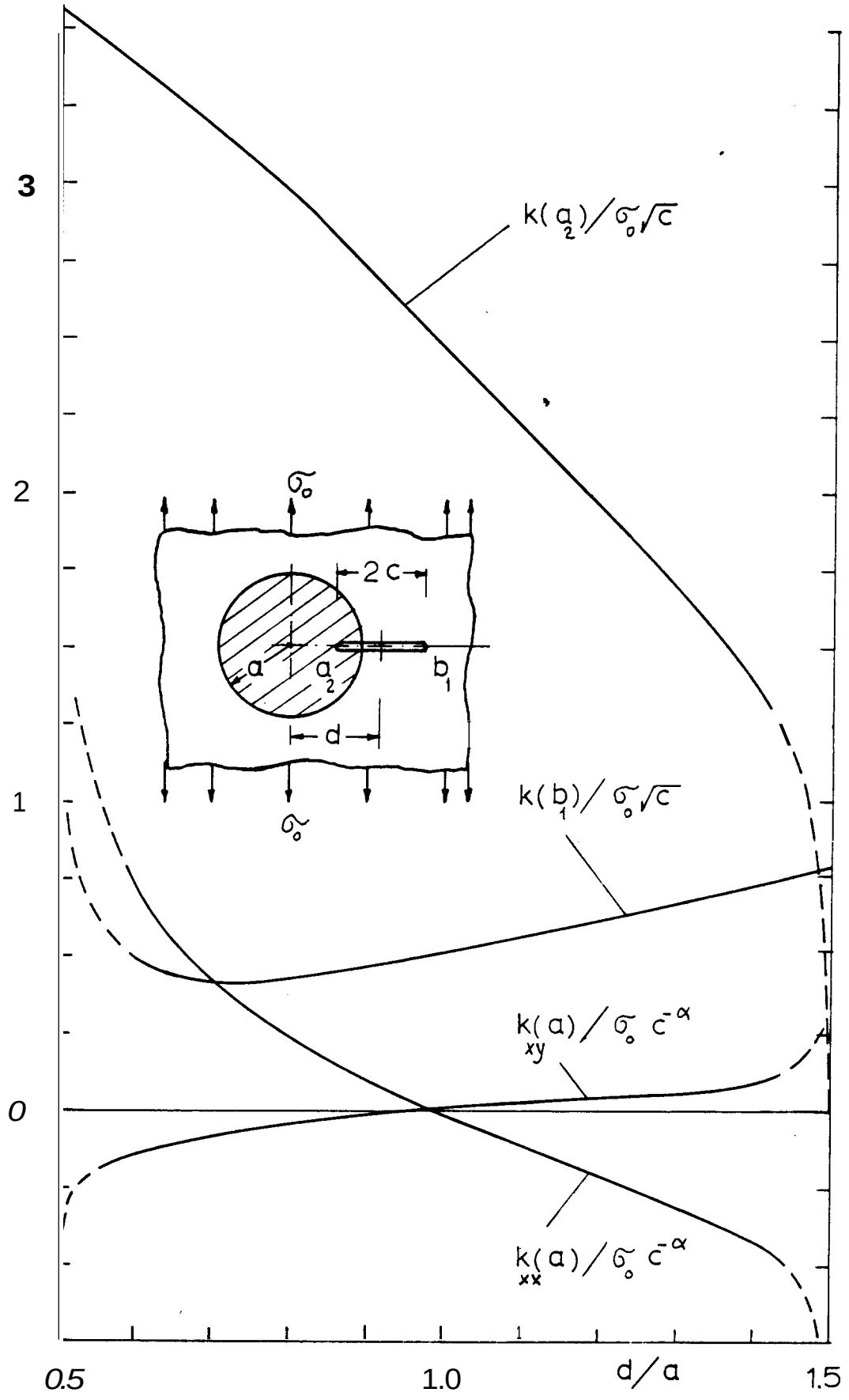

Figure 20. Stress intensity factors for a crack going through the interface ($\kappa_1 = 1.6$, $\kappa_2 = 1.8$, $\mu_2/\mu_1 = 23.077$, $\gamma = \alpha = \beta = 0.27326$, $2c = (b_1 - a_2) = a$ fixed, $d = (b_1 + a_2)/2$ variable).

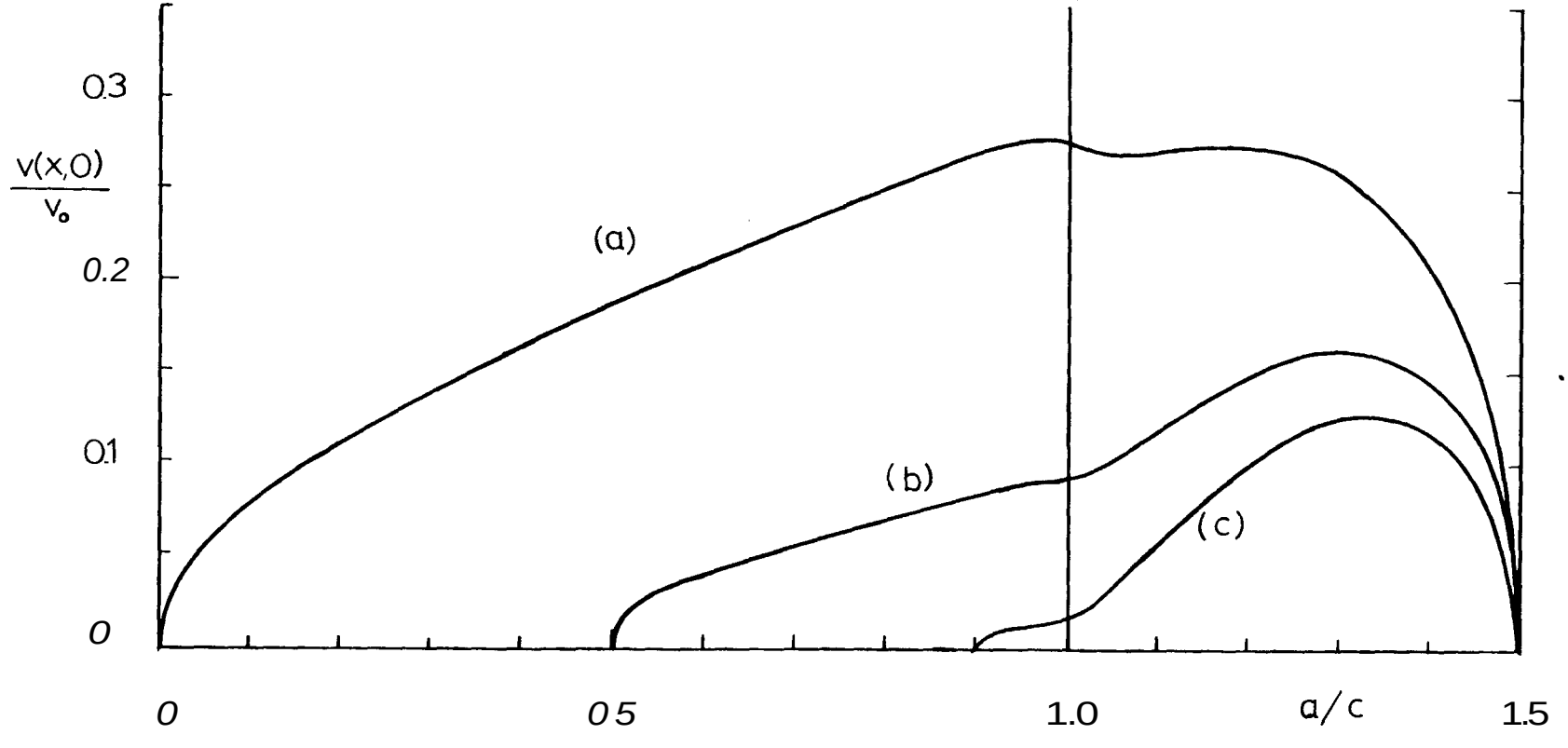

Figure 21. Crack surface displacement for cracks going through the interface ($\kappa_1 = 1.6$, $\kappa_2 = 1.8$, $\mu_2/\mu_1 = 23.077$, $v_0 = (1+\kappa_1)a\sigma_0/\mu_1$, $b_2 = a$ fixed, a_2 variable: (a) $a_2 = 0$, (b) $a_2 = a/2$, (c) $a_2 = 0.9a$).

The asymptotic trends in Fig. 20 can be explained by observing that $\gamma=\alpha=0.27326$ for the crack crossing the boundary $(a_2<b_2=a=a_1<b_1)$, $\alpha=0.5$ for the crack tip embedded in the matrix, $\beta=0.33811$ for the crack in the matrix terminating at the boundary $(a_1=a,\ d/a=1.5)$ and $\alpha=0.82580$ for the crack in the inclusion terminating at the boundary $(b_2=a,\ d/a = 0.5)$.

Figure 21 shows some sample results for the crack surface displacements of a crack crossing the boundary.

For a crack terminating at the boundary to study the further crack propagation the details of the angular variation of the stresses, that is the functions $f_{ij}(\theta)$ in (21) may be needed. Sample results giving the distribution of these functions are shown in Figures 22-24. From the definitions (12), (13) and (21) we note that $f_{\theta\theta}(0) = 1$. The functions G_{ij} shown in Figures 22-24 are obtained from

$$\sigma_{ij}(r,\theta) \tilde{=} \frac{G_{ij}(\theta)}{\sqrt{2}\, r^{\alpha}} \quad , \quad (i,j=r,\theta),\ (-\pi<\theta<\pi). \tag{25}$$

Thus, $G_{\theta\theta}(0) = k(a)$ and $f_{ij}(\theta)$ is given by

$$f_{ij}(\theta) = \frac{G_{ij}(\theta)}{G_{\theta\theta}(0)} \ , \ (i,j=r,\theta) \ , \ (-\pi<\theta<\pi) \quad . \tag{26}$$

The analytical details of a crack terminating at and crossing the boundary in a two-phase nonhomogeneous elastic medium may be found in [14] and [15].

3.2 Anti-Plane Shear Problem for a Crack Interacting with a Circular Inclusion

The simpler problem for a medium containing a crack and a circular elastic inclusion or a hole shown in Fig. 4 and subjected to a uniform anti-plane shear loading

$$\sigma_{yz}(x, \mp \infty) = p_o \tag{27}$$

can also be treated in a manner similar to the plane strain problem

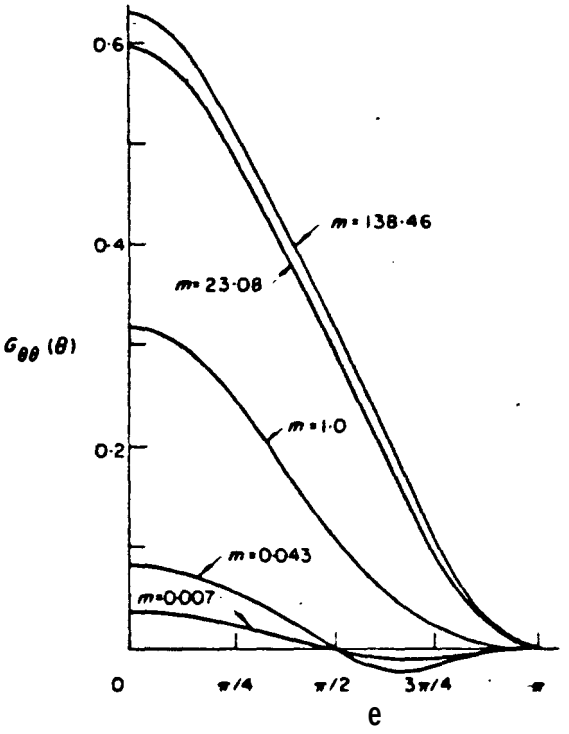

Fig. 22, Angular variation of $\sigma_{\theta\theta}$ **around a** crack tip touching the interface.

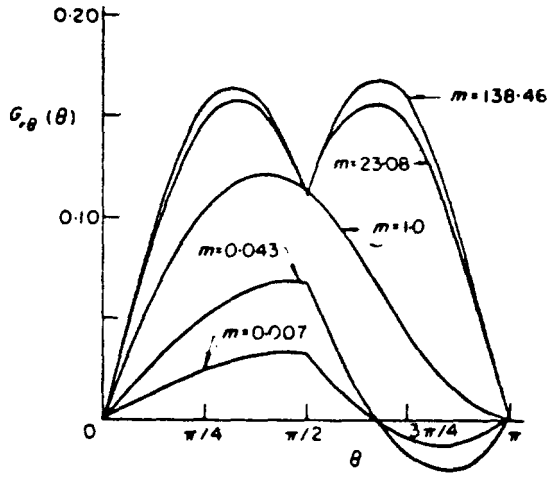

Fig. 23. Angular variation of $\sigma_{r\theta}$ around a crack tip touching the interface.

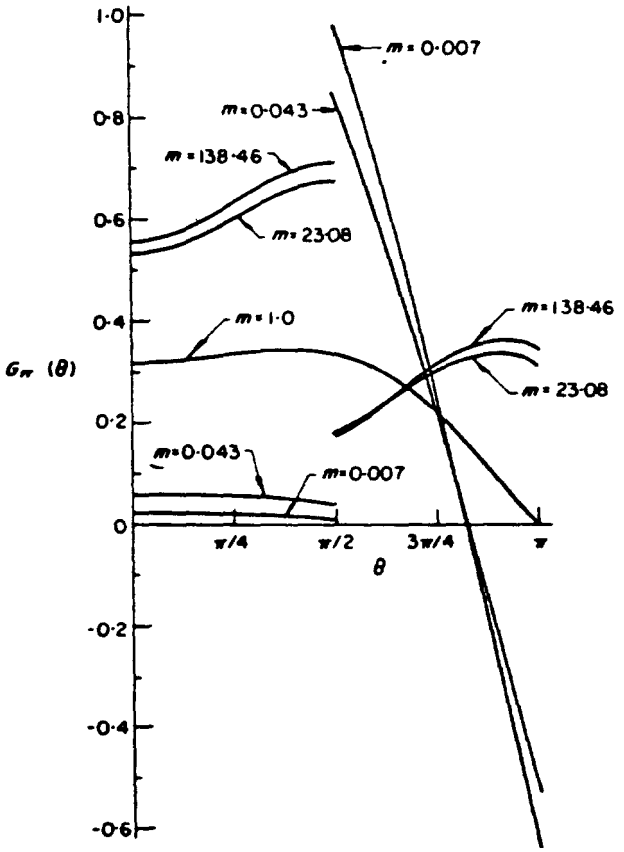

Fig. 24. Angular variation of σ_{rr} around a crack tip touching the interface.

discussed in the previous section. In this case the crack surface tractions for the perturbation problem are obtained by solving the problem of inclusion or hole without a crack. Some sample results giving the stress distribution $\sigma_{yz}(x,y)$ (for various fixed values of y) are shown in Figures 25 and 26. Again note that qualitatively these results are very similar to the plane strain results shown in figures 2 and 5. For this problem some sample results giving the Mode III stress intensity factors k_3 at the crack tips $x = \mp a$ are defined by

$$k(a)p_0\sqrt{a} = k_3(a) = \lim_{x\to a} \sqrt{2(x-a)}\, \sigma_{1yz}(x,c) \quad , \tag{28}$$

$$k(-a)p_0\sqrt{a} = k_3(-a) = \lim_{x+-a} \sqrt{2(x+a)}\, \sigma_{1yz}(x,c) \quad . \tag{29}$$

Figure 27 shows the results for the radial crack in a medium containing an inclusion or a hole. Similar results for an arbitrarily located crack are shown in Figures 28 and 29. Figure 30 gives some comparative results showing the influence of the crack length-to-radius ratio on the stress intensity factors where m is the modulus ratio $m = \mu_2/\mu_1$ and $k(\mp a) = k_3(\mp a)/p_0\sqrt{R}$. For $m = 1$ we have a homogeneous plane with a crack of length 2a for which $k_3(\mp a) = p_0\sqrt{a}$. Consequently

$$k(\mp a) = \frac{k_3(\mp a)}{p_0\sqrt{R}} = \frac{p_0\sqrt{a}}{p_0\sqrt{R}} = \sqrt{a/R} \quad , \tag{30}$$

giving the straight line shown in the figure. For m=0, m=1 and m=23.3 the slopes of $k(\mp a)$ vs. $\sqrt{a/R}$ curves as $(a/R)\to 0$ are 1.47, 1 and 0.57, respectively. The results for m=0 and m>0 are obtained from the solution of an "infinite" plane with a central crack subjected to the crack surface tractions $\sigma_{yz}(x,0)$ which are equal and opposite to the corresponding stresses given in figures 25 and 26 at x=b=1.5R.

The singular behavior of the stresses terminating at and crossing the boundary is discussed in [16] and [17].

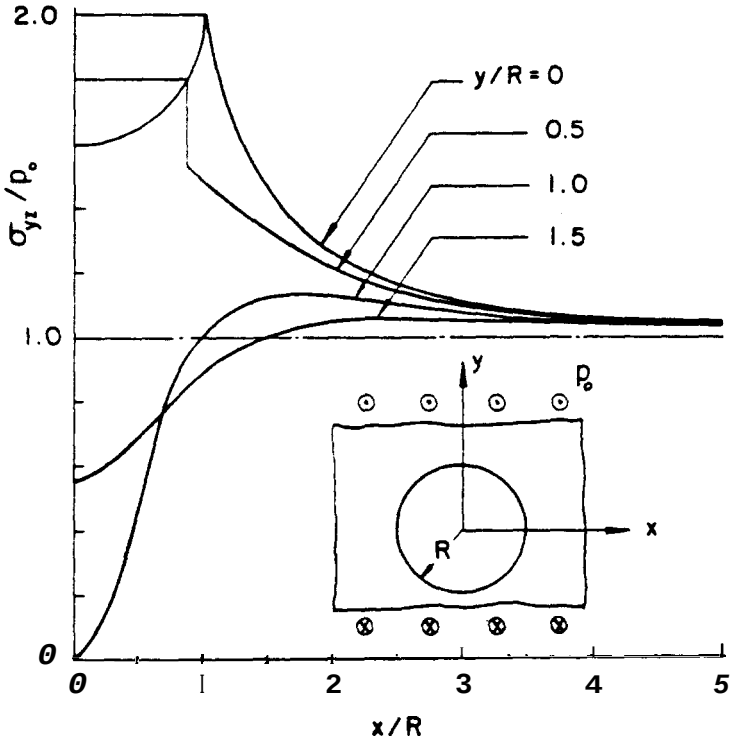

Fig. 25. The shear stress τ_{yz} in a matrix with a circular hole.

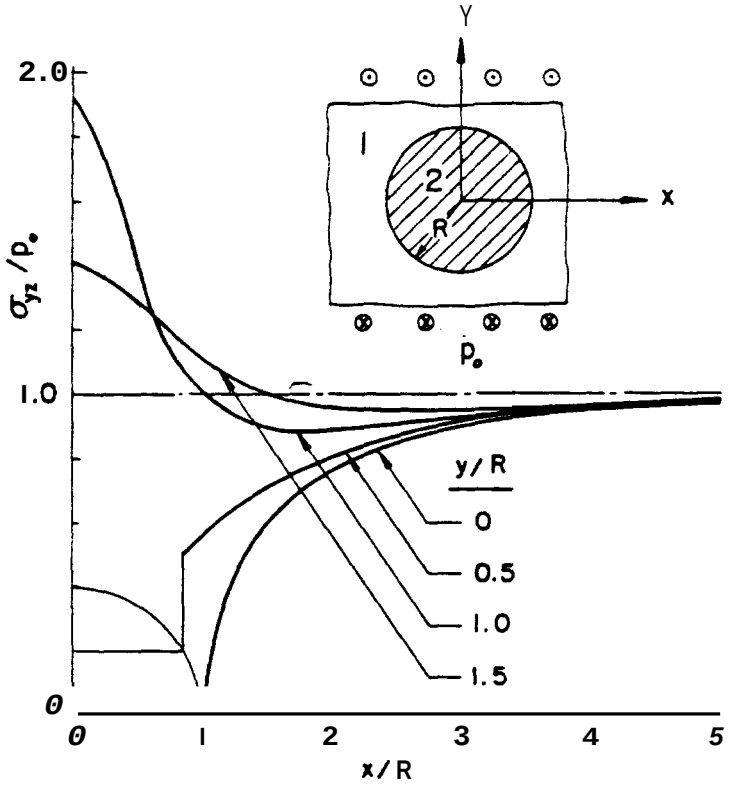

Fig. 26. The shear stress τ_{yz} in a matrix with a circular inclusion ($\mu_2 = 23.3\ \mu_1$).

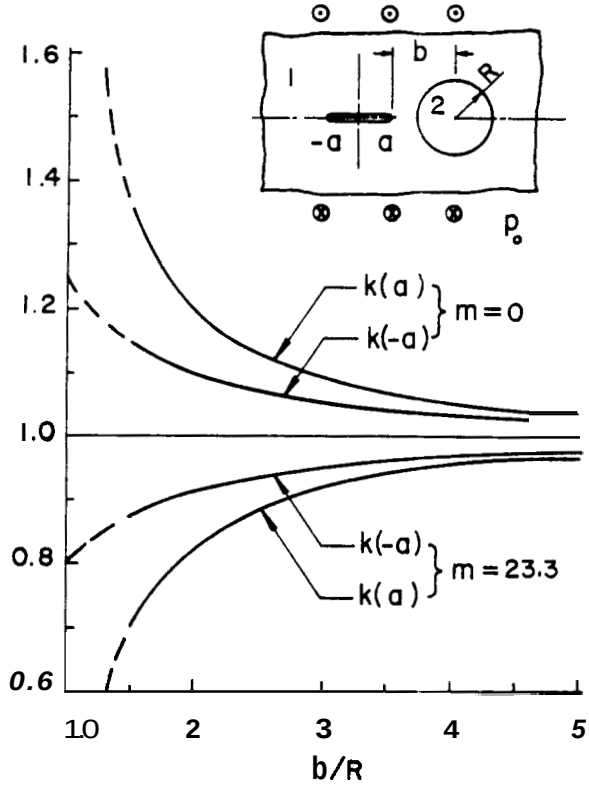

Fig. 27. Stress intensity factors for the antiplane shear problem ($k = k_3/p_0\sqrt{a}$, $R = a$).

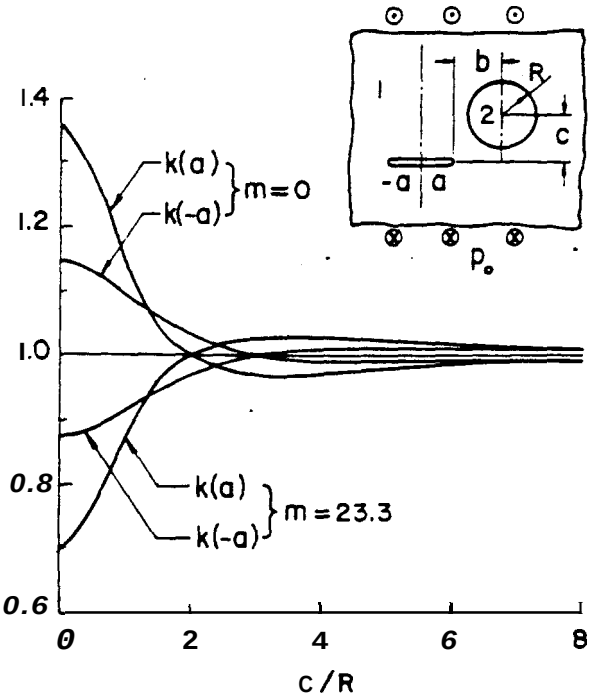

Fig. 28. Stress intensity factors for the antiplane shear prohlem ($k=k_3/p_0\sqrt{a}$, R=a, b=1.5R).

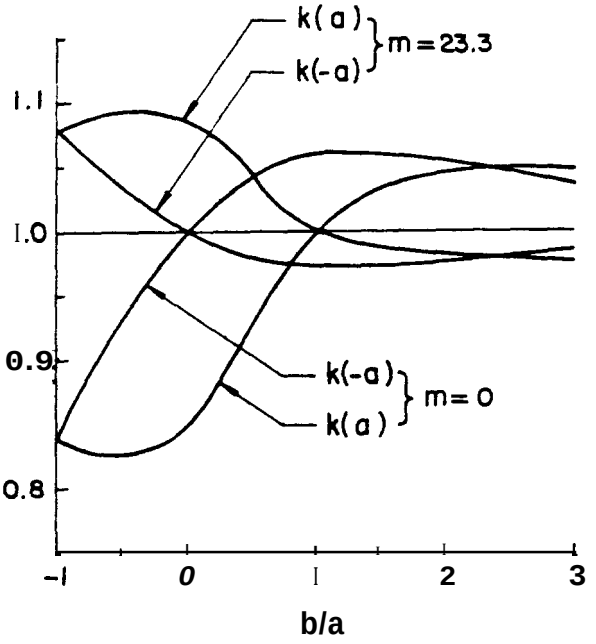

Fig. 29. Stress intensity factors for the antiplane shear prablem ($k=k_3/p_0\sqrt{a}$, R=a, c=1.5R).

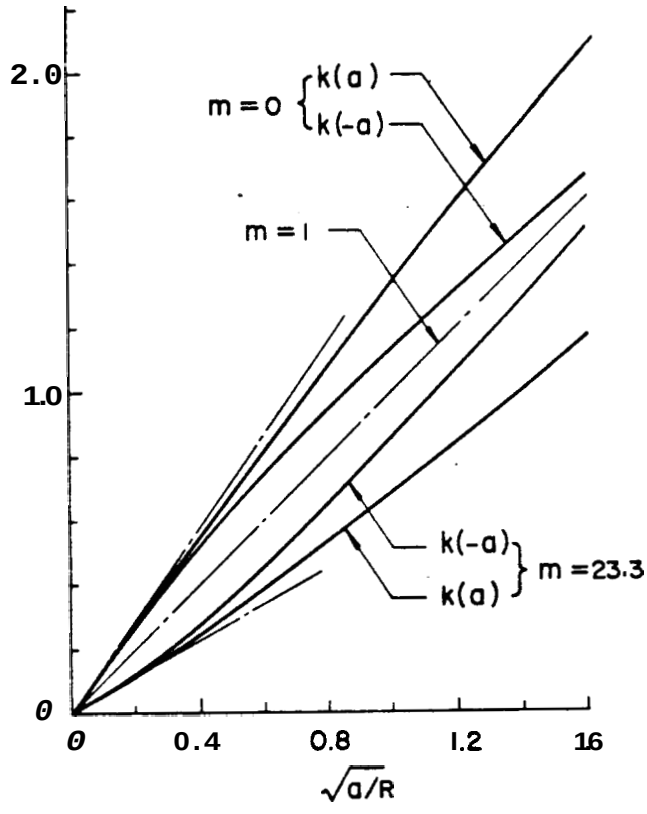

Fig. 30. **Stress** intensity factors for the antiplane shear problem ($k=k_3/p_0\sqrt{R}$, $c=0$, $b=1.5R$).

4. INTERACTION BETWEEN CRACKS

In this section the problem of interaction between cracks on the surface and inside a plate with finite thickness is considered.

4.1 Interaction Between Parallel Internal Cracks

The basic geometry of the problem is shown in Fig. 31. In this section we will consider various special cases relating two or three cracks on the surface of a plate under uniform tension.

For two symmetrically located parallel cracks the stress intensity factors are given in Table 3. Referring to Fig. 31, for this problem we have a=b (i.e., no crack on X axis) c = H-d, P = 0 (no concentrated force) 2B is the distance between the cracks, 2ℓ is the crack length and $\sigma_{YY} = \sigma_0$ for $y \to \mp\infty$. In this section too the Modes I and II stress intensity factors k_1 and k_2 are defined by

$$k_1 = \lim_{r\to 0} \sqrt{2r}\, \sigma_{yy}(r,0) \quad , k_2 = \lim_{r\to 0} \sqrt{2r}\, \sigma_{xy}(r,0) \quad , \tag{31}$$

where r,ϕ are the polar coordinates at the crack tip, the crack being along $\phi = \pi$. Note that as the distance 2B between the cracks decreases k_1 also decreases and k_2 becomes more significant. The angle θ shown in this table is an (approximate) direction of a probable crack growth which is obtained from a simple assumption that along this radial line at the crack tip the cleavage stress $\sigma_{\theta\theta}(r,\theta)$ is maximum [12], where $r<<H-d$. Here $\theta>0$ indicates that the cracks would grow away from each other.

4.2 Interaction Between Parallel Surface Cracks

The stress intensity factors and the angle of probable crack growth direction in a plate containing two parallel and equal surface cracks under uniform tension or pure bending are shown in Figures 32-35. In this problem we have a=b, c=0 and d<H. The figures also show the Mode I

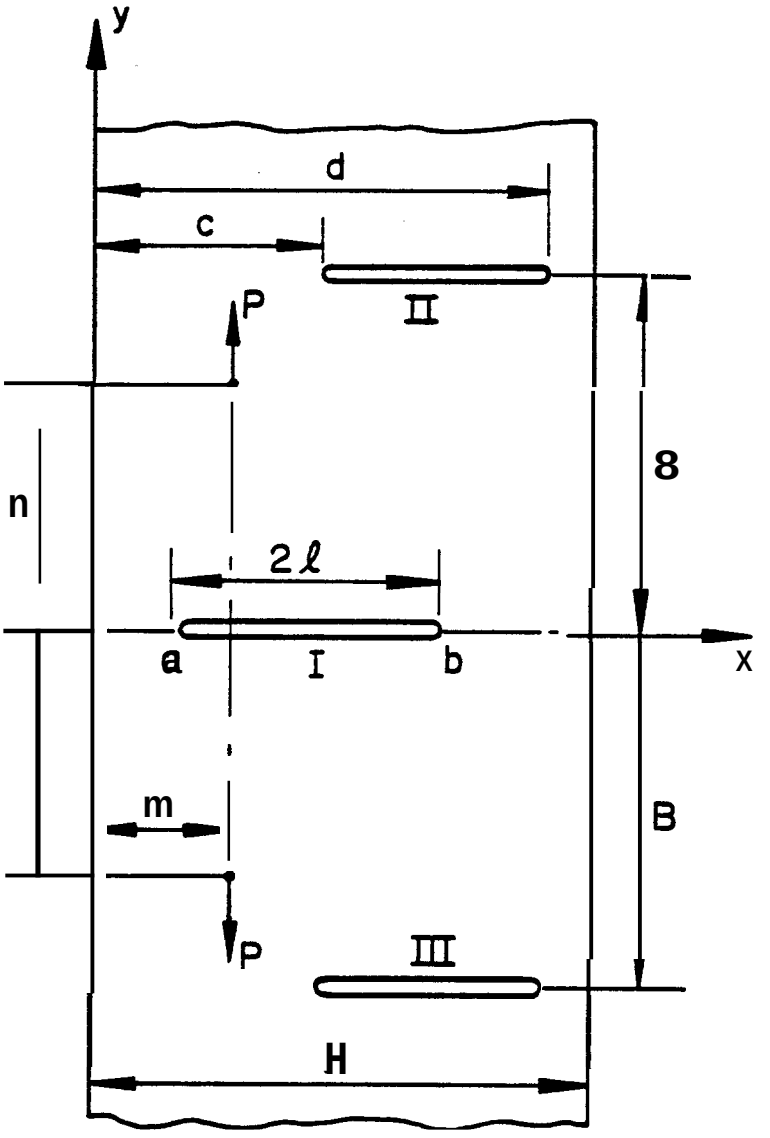

Figure 31. The basic crack geometry.

Table 3. **Stress** intensity factors in a strip containing **two** symmetric internal cracks, $\ell=(d-c)/2$.

ℓ/H	B/ℓ	$k_1/\sigma_0\sqrt{\ell}$	$k_2/\sigma_0\sqrt{\ell}$	$\theta(°)$
0.05	0.5	0.7797	–0.1175	16.430
	1.0	0.8512	–0.0616	8.194
	1.5	0.9052	–0.0308	3.887
	2.0	0.9395	–0.0163	1.992
	5.0	0.9953	–0.0001	0.157
	10.0	1.0053	–0.00001	0.014
	20.0	1.0060	0.0000	0.000
0.1	0.5	0.7992	–0.1199	16.363
	1.0	0.8749	–0.0624	8.076
	1.5	0.9310	–0.0307	3.774
	2.0	0.9660	–0.0162	7.920
	5.0	7.0219	–0.0001	0.106
	10.0	1.0247	–0.00001	0.003
	20.0	1.0248	0.0000	0.000
0.2	0.5	0.8846	–0.2570	15.578
	1.0	0.9749	–0.0656	7.634
	1.5	1.0437	–0.0330	3.648
	2.0	1.0839	–0.0155	1.641
	5.0	1.1096	–0.0001	0.019
	10.0	7.1097	0.0000	0.000

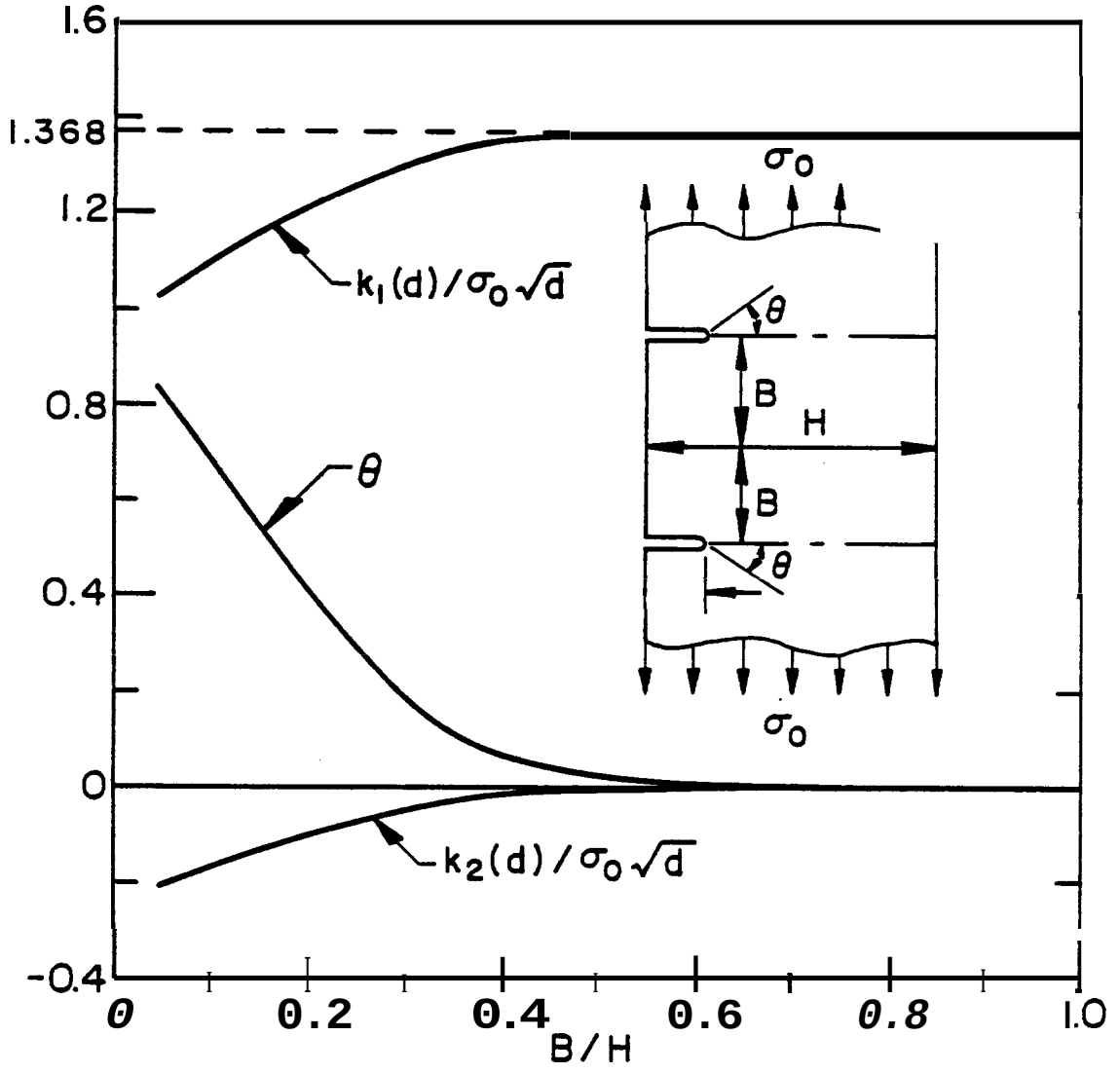

Figure 32. Stress intensity factors and probable crack propagation angle in an infinite strip containing two edge cracks under uniform tension, d=0.2H.

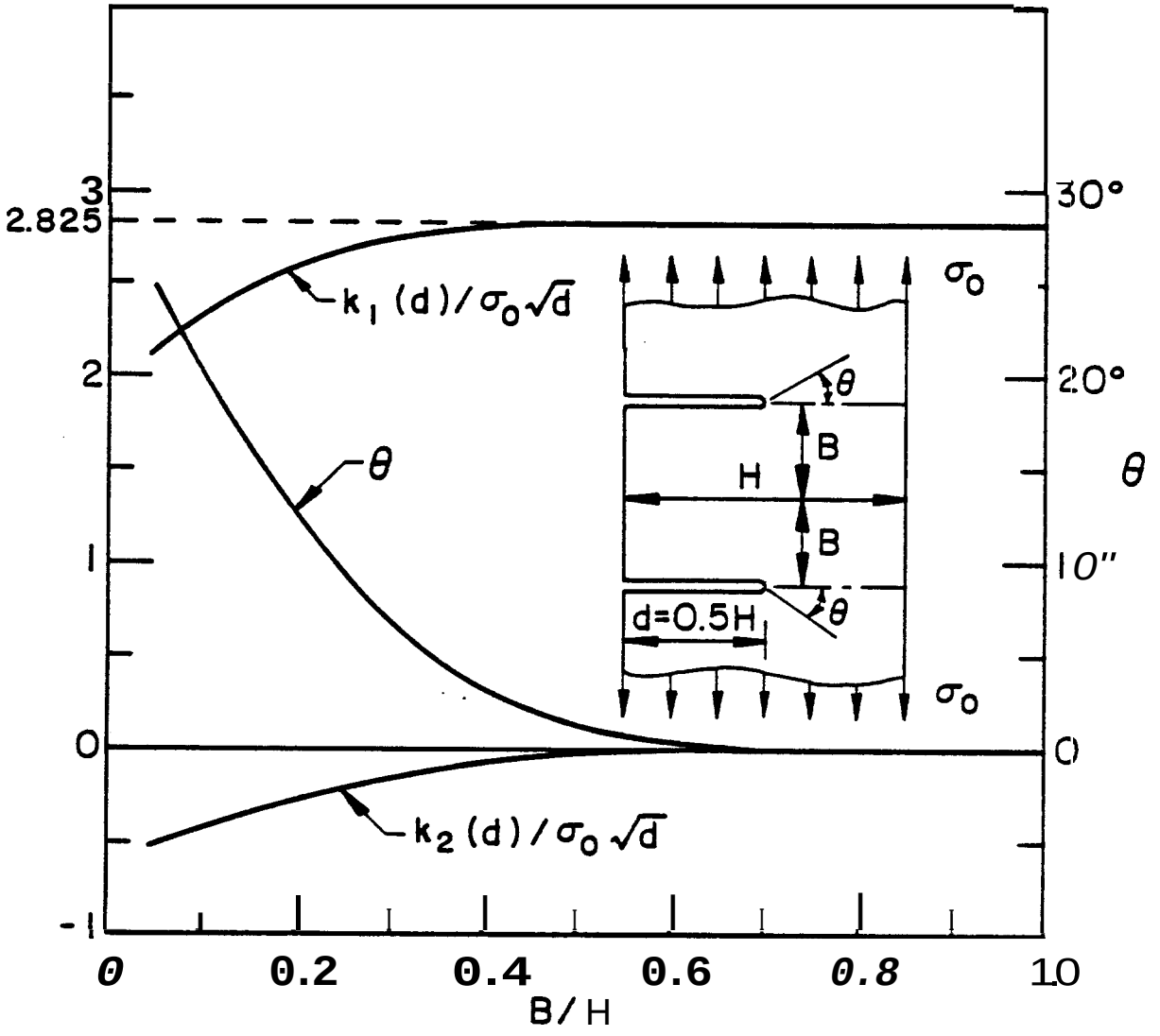

Figure 33. Same as Figure 2, d=0.5H.

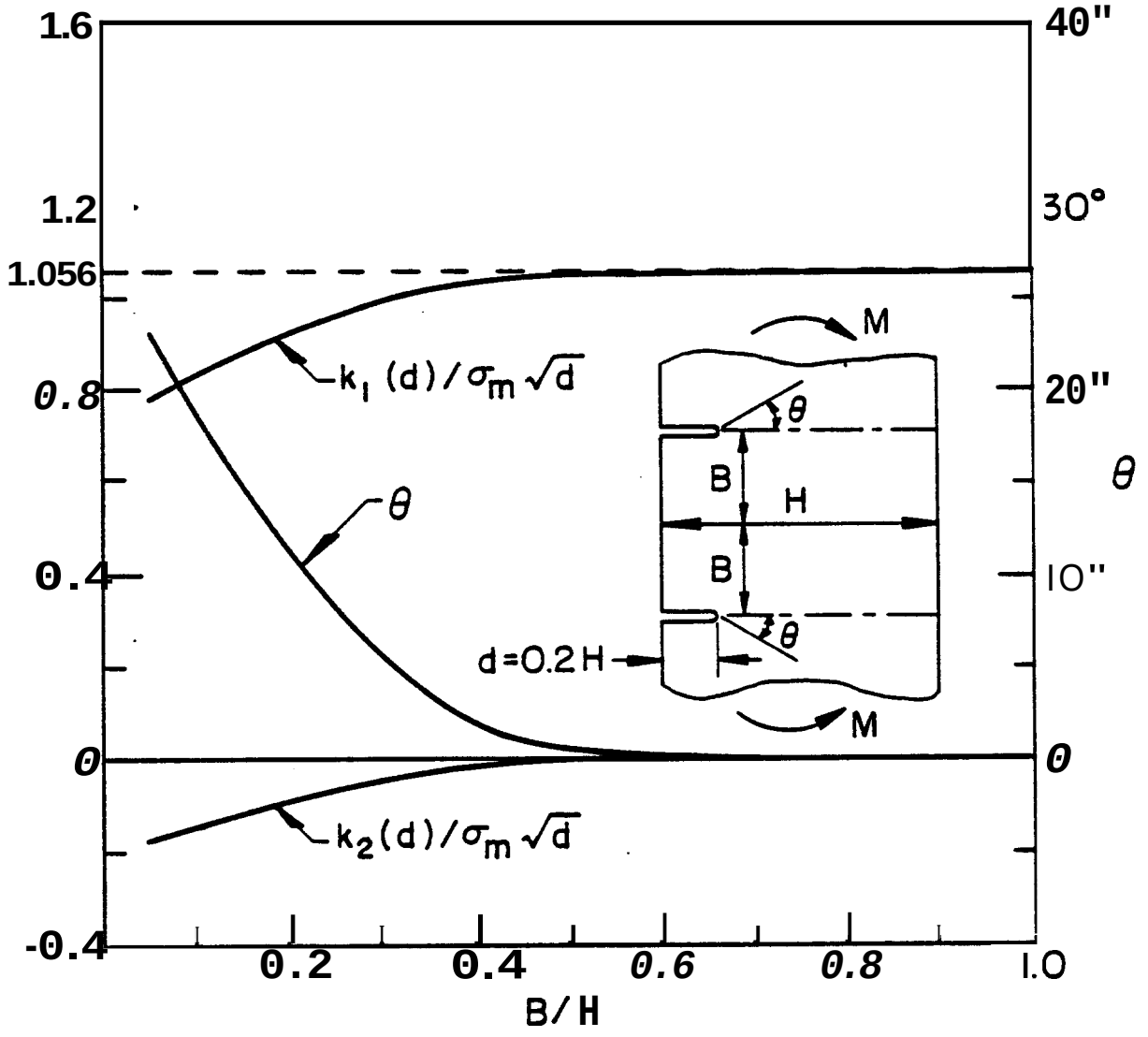

Figure 34. Stress intensity factors and probable crack propagation angle in an infinite strip with two edge cracks under bending, d=0.2H.

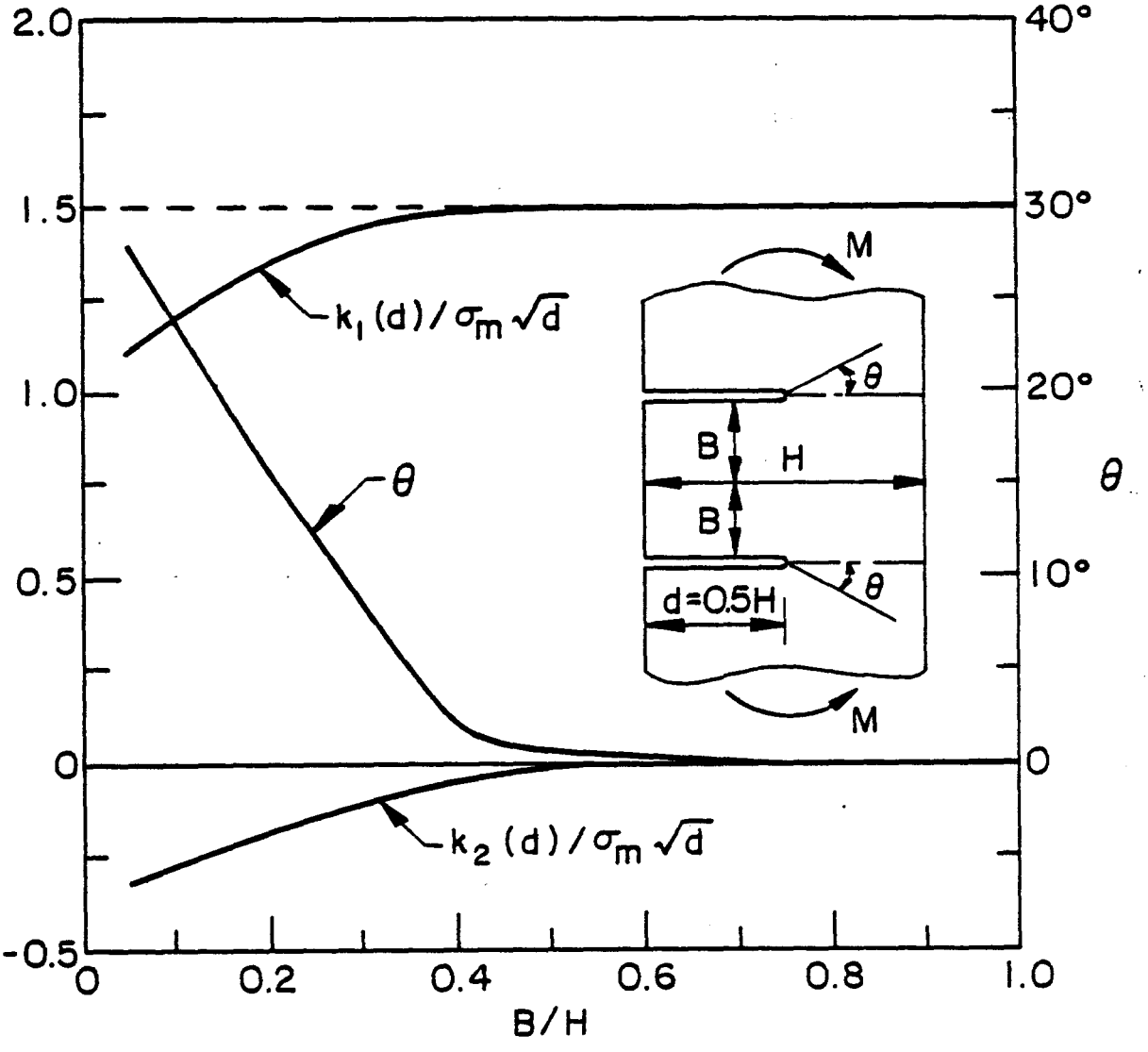

Figure 35. Same as Figure 4, d=0.5H.

stress intensity factor k_1 for a single surface crack for comparison (the dashed line). For the single crack k_2 is 0. Again note that k_1 is smaller than the corresponding single crack value, k_2 becomes more significant as B decreases, and cracks would tend to propagate away from each other. For the bending problem shown in Figures 34 and 35 the normalizing stress σ_m is given by

$$\sigma_m = \frac{6M}{H^2} \tag{32}$$

where M is the moment for unit thickness.

Figures 36–41 show the results for a plate containing three parallel surface cracks under uniform tension or bending. In this case, too, $k_2<0$, meaning that the outside cracks would grow away from the middle crack. Comparison of the two and three crack results shows that the introduction of the middle crack "relaxes" the stress intensity factors in the outer cracks. Fig. 40 shows that for short cracks the interaction and for longer cracks the back surface effect would dominate. Figure 41 shows the results for three point bending. In this problem, too, σ_m is the surface stress in the plate under bending, namely

$$\sigma_m = \frac{6M}{H} = \frac{24P}{H} \quad . \tag{33}$$

The stress intensity factor k(d) for the outer cracks approaches zero as $B \to 4H$ (for which the moment is zero).

4.3 Cracks Parallel to the Boundary

The basic geometry for the plate containing a crack parallel to the boundary is shown by the insert in Fig. 42. The problem considered in this section also takes into account the material orthotropy. Thus, the material constants shown in Fig. 42 are related to the elastic constants of an orthotropic plate as follows:

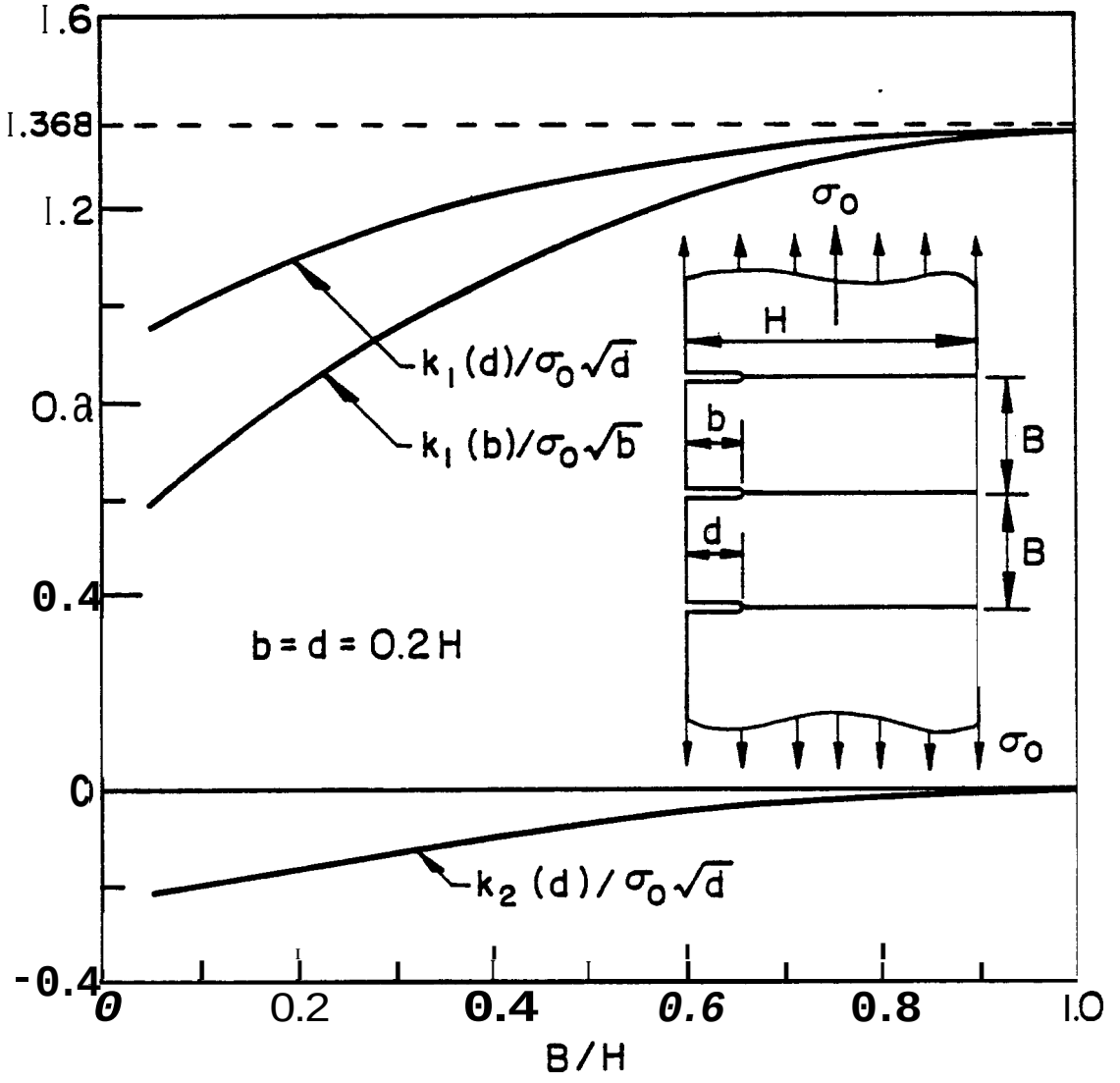

Figure 36. Stress intensity factors in an infinite strip containing three edge cracks under uniform tension, d=b=0.2H.

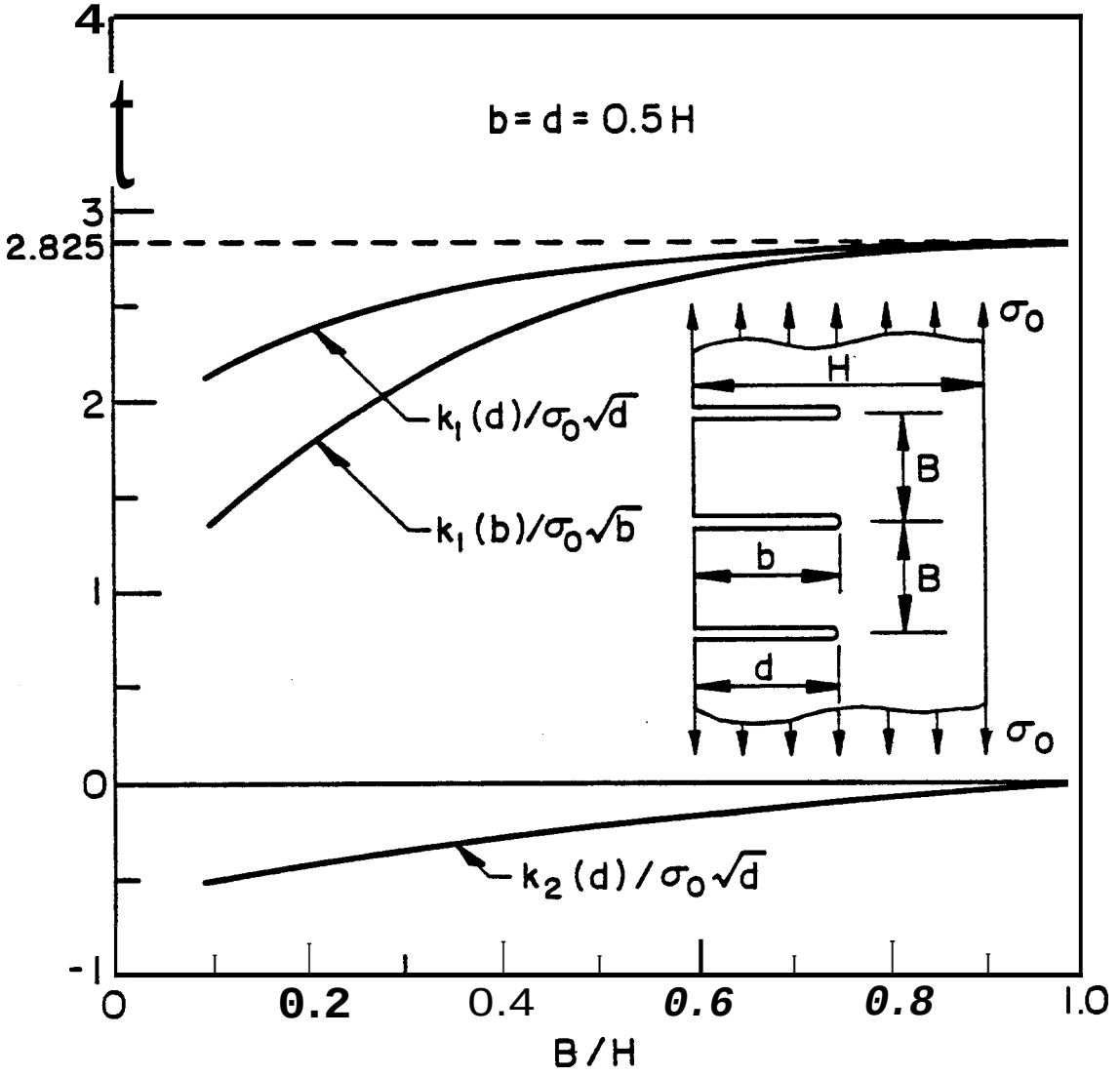

Figure 37. Same as Figure 6, d=b=0.5H.

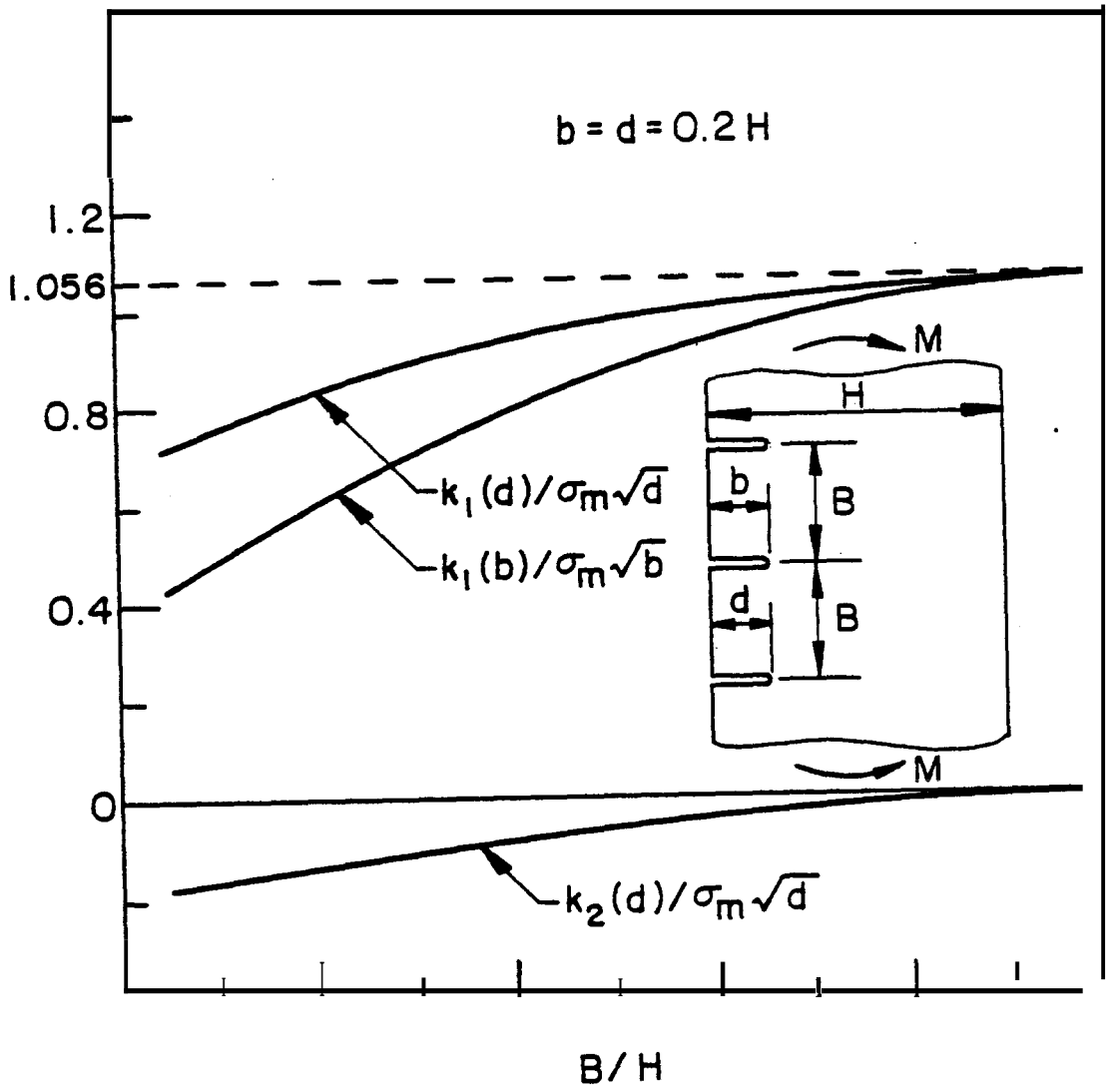

Figure 38. **Stress** intensity factors in an infinite strip containing **three** edge cracks under bending, $d=b=0.2H$, $\sigma_m=6M/H^2$.

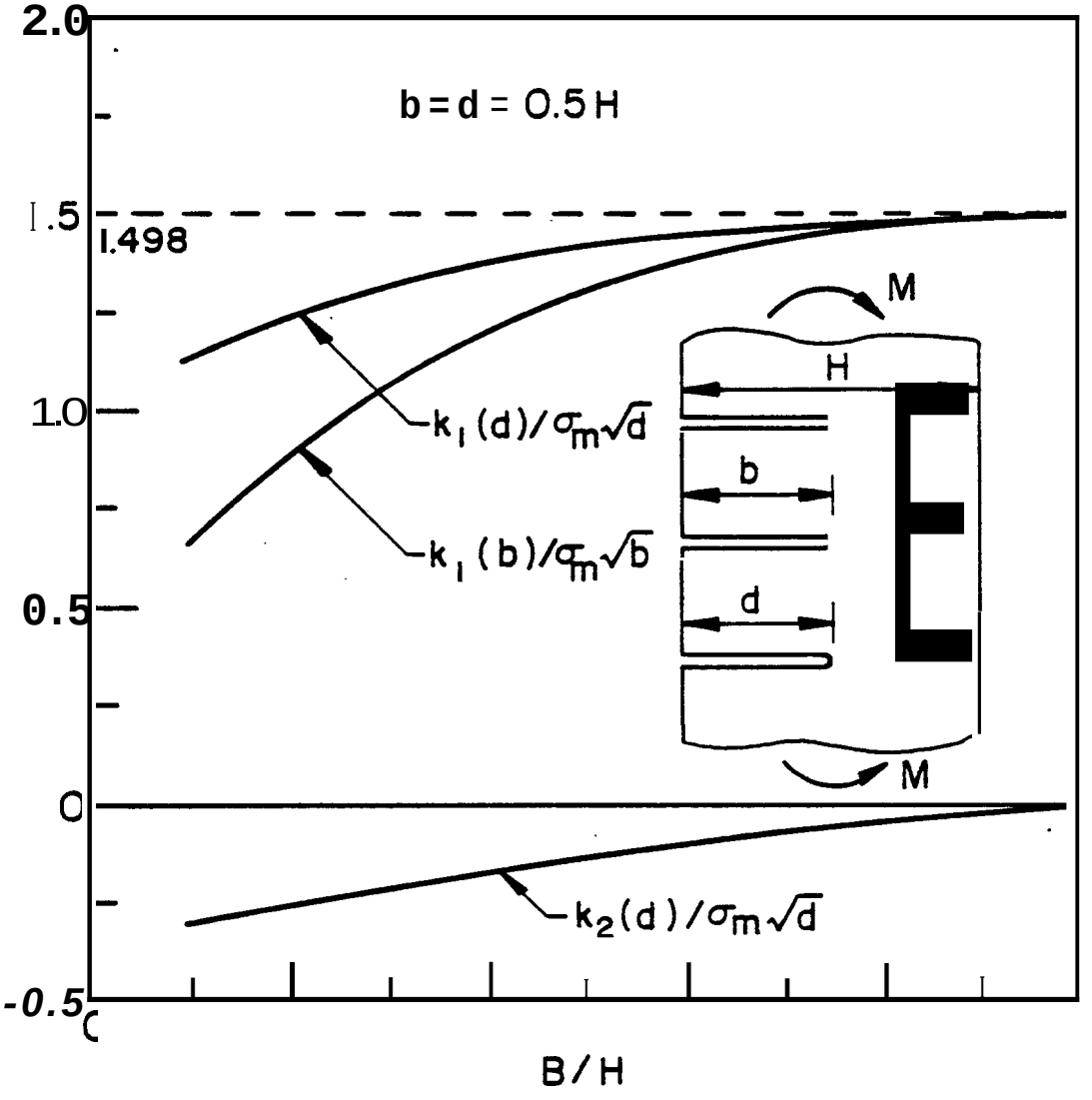

Figure 39. Same as Figure 8, d=b=0.5H, $\sigma_m=6M/H^2$.

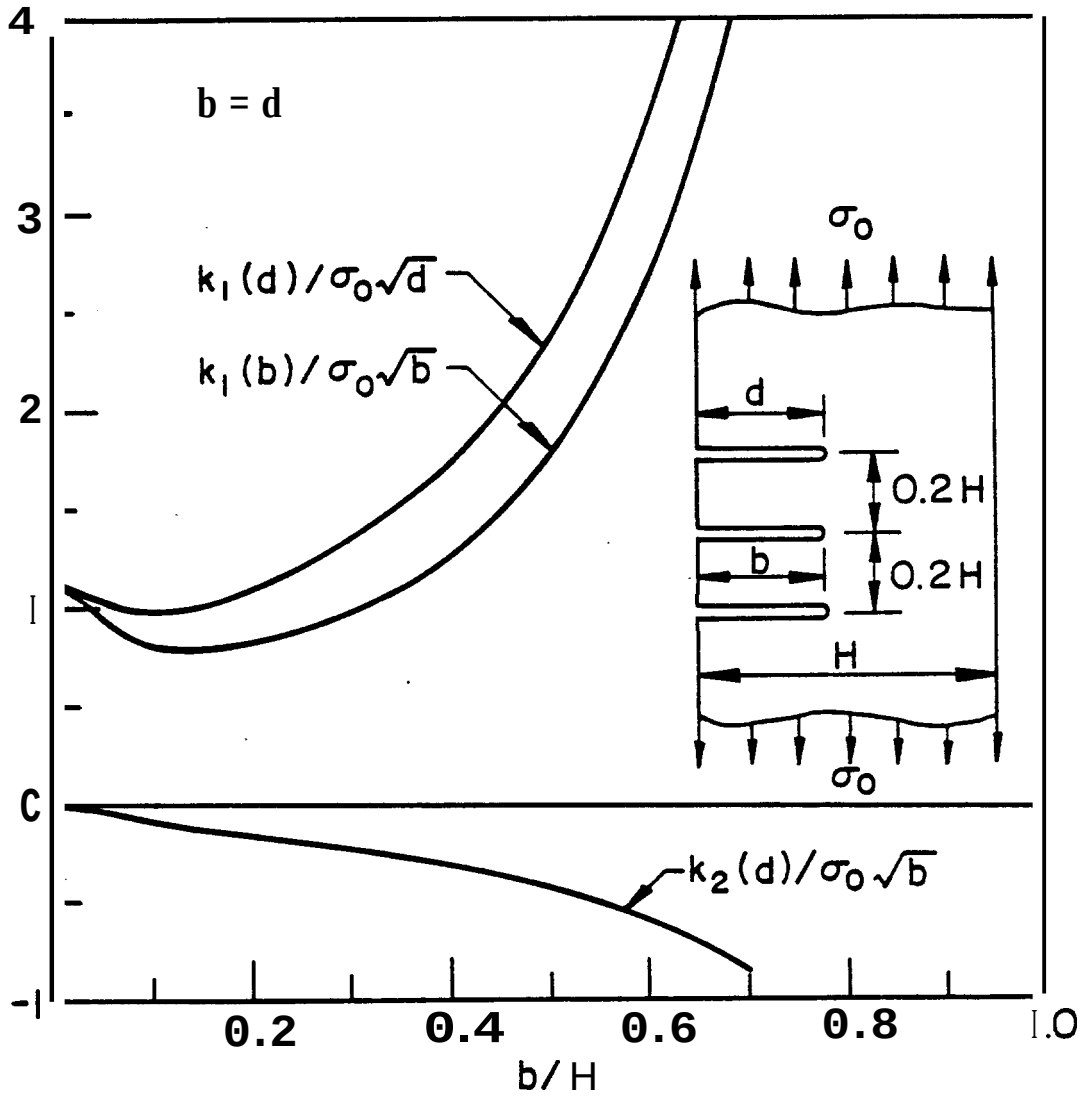

Figure 40. The effect of the crack depth on the stress intensity factors in an infinite strip under tension, B=0.2H.

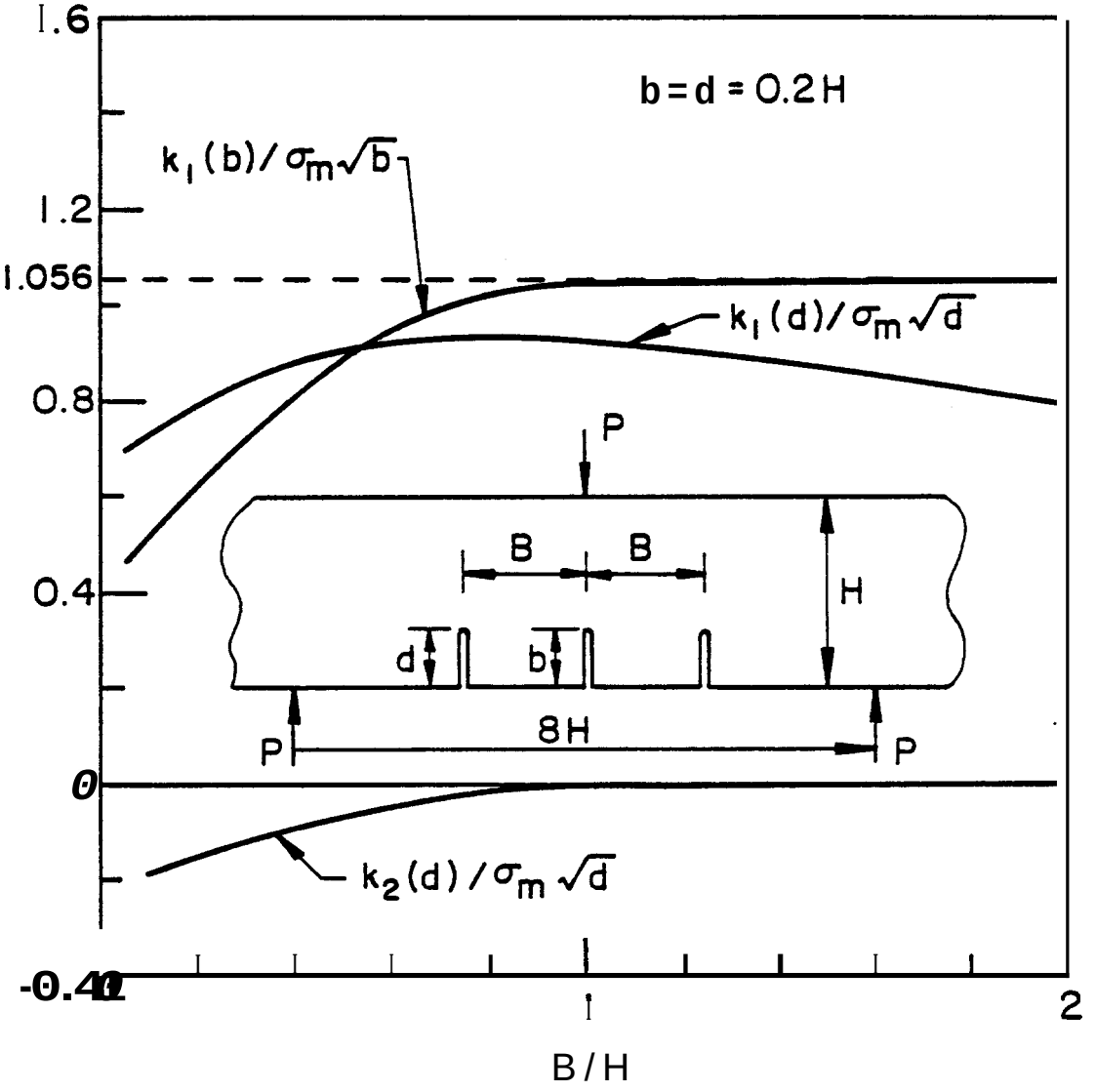

Figure 41. Stress intensity factors in an infinite strip containing edge cracks and subjected to three point bending, $\sigma_m = 6M/H^2 = 24P/H$.

$$\delta^4 = E_{11}/E_{22} \quad , \quad \kappa = \frac{\sqrt{E_{11}E_{22}}}{2G_{12}} - \sqrt{\nu_{12}\nu_{21}} \quad . \tag{34}$$

The engineering material constants which appear in (34) are defined by the following stress-strain relations

$$\begin{aligned} \varepsilon_{11} &= \frac{1}{E_{11}}(\sigma_{11} - \nu_{12}\sigma_{22} - \nu_{13}\sigma_{33}) \ , \ \cdots \\ 2\varepsilon_{12} &= \frac{1}{G_{12}}\tau_{12} \ , \ \cdots \end{aligned} \tag{35}$$

In Fig. 42 and the subsequent figures the coordinate axes 1 and 2 are respectively parallel and are perpendicular to the crack. The main result of Fig. 42 is that as the crack approaches the boundary the stress intensity factors become unbounded. Also, the analysis of the mixed mode stress state at the crack tip would indicate that the direction along which the cleavage stress is maximum is inclined toward the nearest boundary, meaning that any further propagation of the crack would be toward the nearest boundary. The corresponding results for a crack loaded under pure shear are shown in Fig. 43. The peculiarity of these results is that the Mode II stress intensity factor is relatively insensitive to the location of the crack, in fact it somewhat decreases as the crack approaches the boundary before becoming unbounded.

Figures 44 and 45 show the effect of the relative crack length for a symmetrically located crack under Modes I and II loading conditions.

The results for two collinear cracks loaded under Mode I conditions are shown in Fig. 46. The figure also shows the stress intensity factors for an infinite plate (H=∞) which are given by

$$k_1(b) = p\sqrt{(b-a)/2}\,\left(\frac{2b}{b-a}\right)^{1/2}\left[1 - \frac{E(k)}{K(k)}\right]/k \tag{36}$$

$$k_1(a) = p\sqrt{(b-a)/2}\,\left(\frac{2b^2}{a(b-a)}\right)^{1/2}\left[\frac{E(k)}{K(k)} - \left(\frac{a}{b}\right)^2\right]/k \tag{37}$$

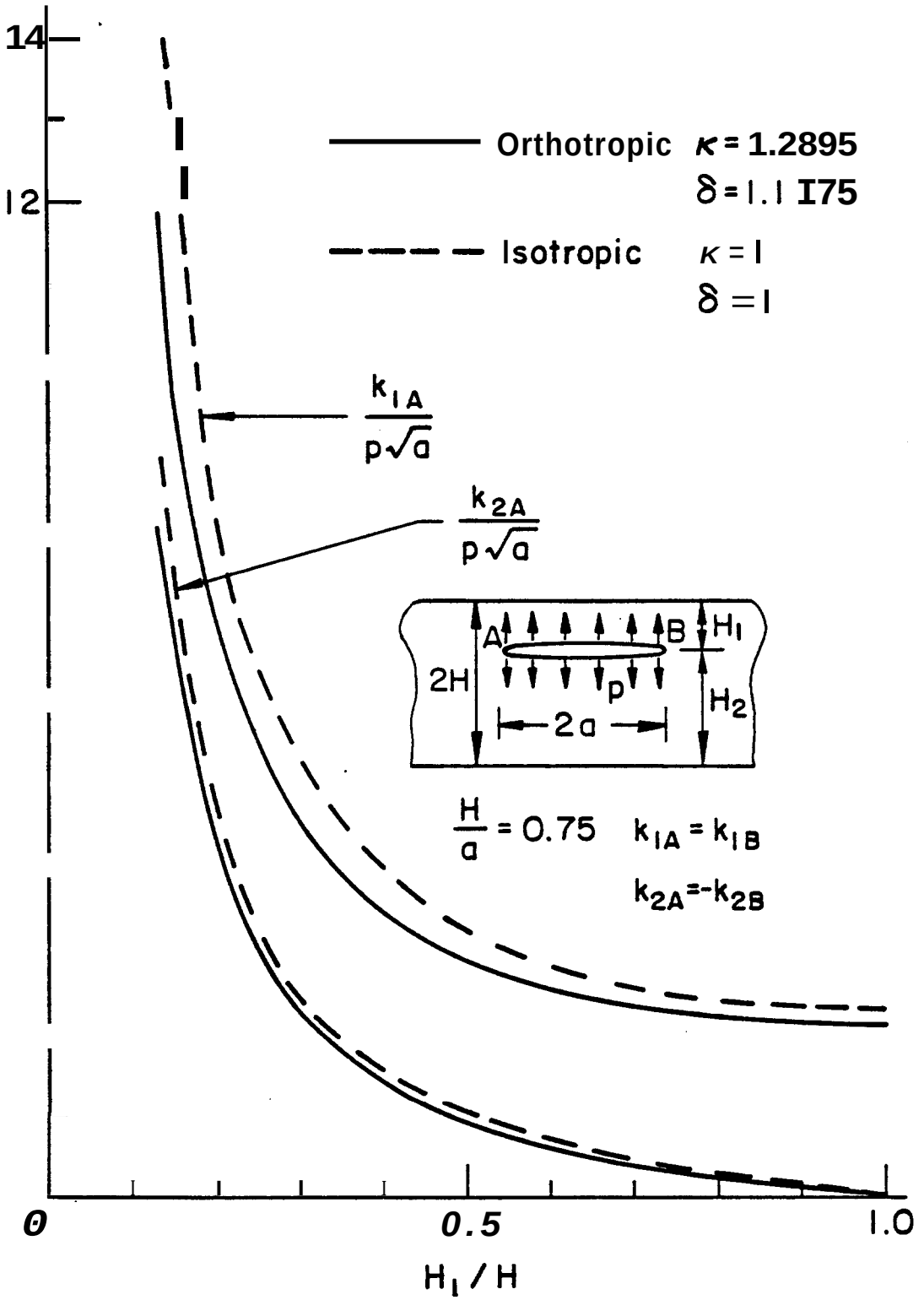

Figure 42. The effect of the crack location on the stress intensity factors for uniform surface pressure. H = 0.75a, $\delta = 1 = \kappa$ for the isotropic materials and $\delta = 1.1175$, $\kappa = 1.2895$ for the orthotropic material (yellow birch).

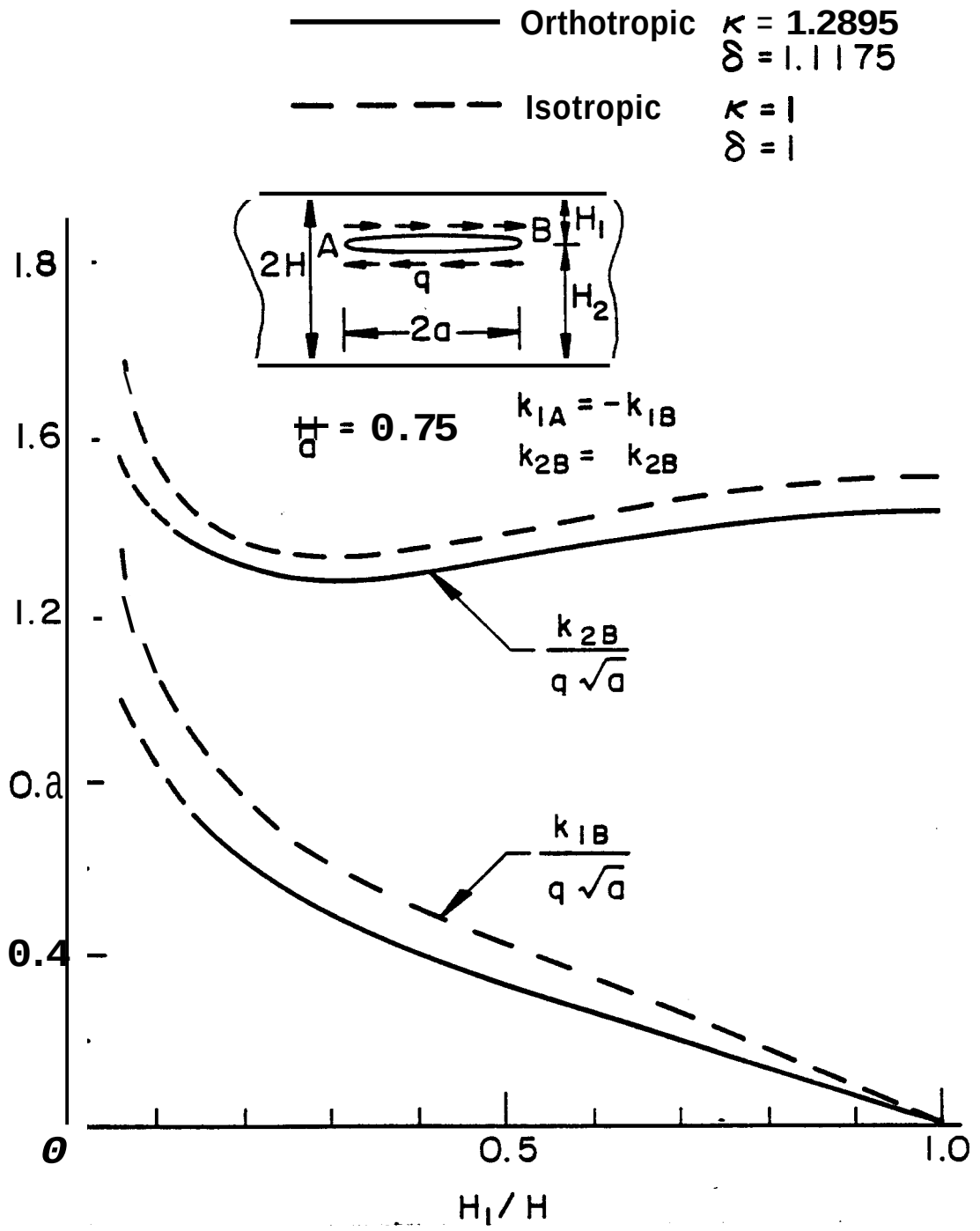

Figure 43. Same as figure 2 for uniform shear applied to the crack surface.

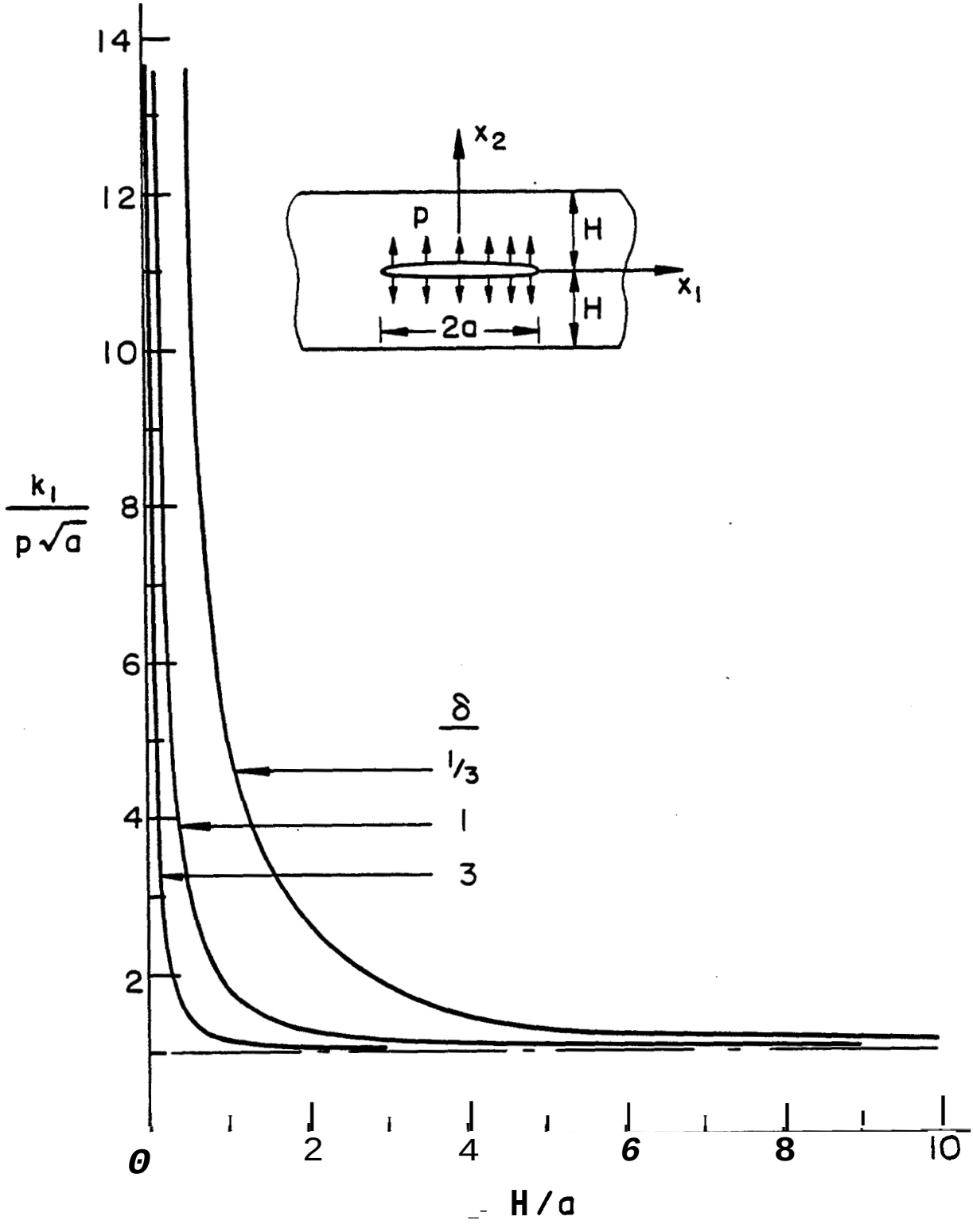

Figure 44. Effect of the crack length on the stress intensity factor for a symmetrically located crack under uniform pressure, $\kappa = 1$.

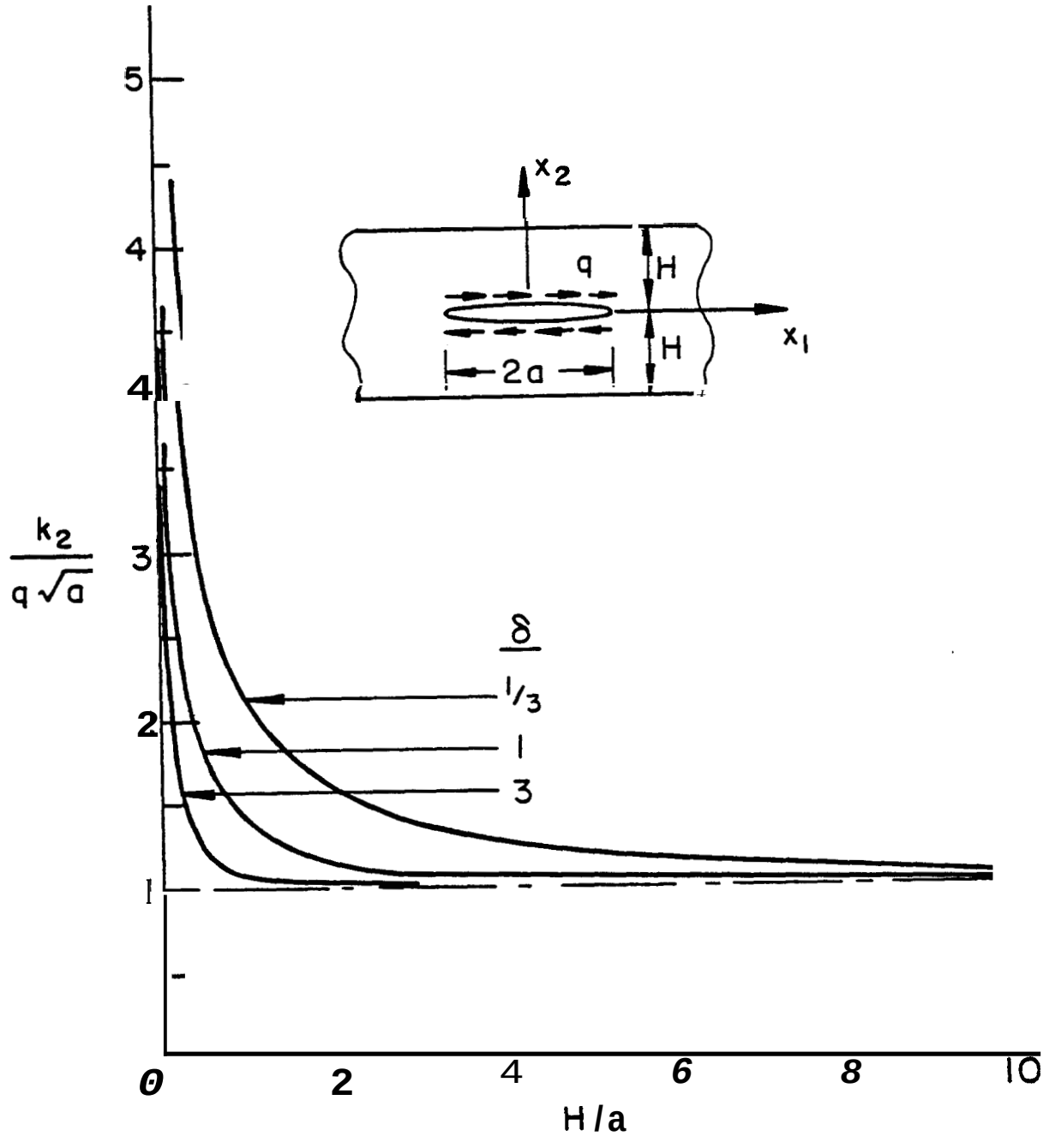

Figure 45. **Same as** figure **4** for uniform **shear applied** to **crack surface.**